Fast MAS ^{1}H NMR Study of Water Adsorption and Dissociation On the (100) Surface of Ceria Nanocubes: A Fully Hydroxylated, Hydrophobic Ceria Surface

Journal:	*The Journal of Physical Chemistry*
Manuscript ID	jp-2016-12375c.R1
Manuscript Type:	Article
Date Submitted by the Author:	n/a

Complete List of Authors:	Gill, Lance; Bruker BioSpin Corp, Beste, Ariana; Joint Institute for Computational Sciences Chen, Banghao; Florida State University, Chemistry & Biochemistry Department Li, Meijun; Oak Ridge National Laboratory, Chemical Sciences Division Mann, Amanda; Merck and Co., Analytical Sciences Overbury, Steven; Oak Ridge National Laboratory, Chemical Sciences Division Hagaman, Edward; Oak Ridge National Laboratory, Chemical Sciences Divsion

Fast MAS ^{1}H NMR Study of Water Adsorption and Dissociation On the (100) Surface of Ceria Nanocubes: A Fully Hydroxylated, Hydrophobic Ceria Surface

Lance Gill [a], Ariana Beste [b], Banghao Chen [a], Meijun Li [a], Amanda K. P. Mann [a], Steven H. Overbury [a] and Edward W. Hagaman [a] *

[a] Chemical Sciences Division, Oak Ridge National Laboratory, Oak Ridge, Tennessee, 37831

[b] Joint Institute for Computational Sciences, The University of Tennessee, Oak Ridge, TN 37831

Fast MAS ^{1}H NMR Study of Water Adsorption and Dissociation On the (100) Surface of Ceria Nanocubes: A Fully Hydroxylated, Hydrophobic Ceria Surface

Abstract.

^{1}H nuclear magnetic resonance (NMR) spectroscopy was used to study hydroxylic surface species on ceria nanocubes, a crystalline, high surface area CeO_2 that presents mostly (100) facets. Water adsorption and desorption experiments in combination with fast magic angle spinning (MAS, 20-40 kHz) ^{1}H NMR provide high resolution ^{1}H spectra that allow the observation of ten resonance bands (water or hydroxyl) on or under the (100) surface. Assignments were made using a combination of adsorption and temperature-programmed desorption, quantitative spin counting, deuterium exchange, spin-lattice (T_1) and spin-spin (T_2) relaxation, and DFT calculations. In air the (100) surface exists as a fully hydroxylated surface. Water adsorption and dissociation on dry ceria surfaces occur first at oxygen vacancies, but Ce^{3+} centers are not required since water dissociation is barrier-less on the fully oxidized surface. Surface –OH functionality occurs in two resolved bands representing isolated –OH (1 ppm) and hydrogen-bonded –OH (9 ppm), the latter being dominant. Deuterium exchange of surface hydroxyls with D_2O does not occur under mild or forcing conditions. Despite large differences in the T_1 of surface hydroxyls and physisorbed water, surface hydroxyl T_1 values are independent of the presence or absence of physisorbed water, demonstrating that the protons within these two functional group pools are not in intimate contact. These observations show that, once hydroxylated, the surface –OH functionality preferentially form hydrogen bonds with surface lattice oxygen, i.e., *the hydroxylated (100) surface of ceria is hydrophobic*. Near this surface it is energetically more favorable for physisorbed water to hydrogen bond to itself rather than to the surface. DFT

calculations support this notion. Impurity Na^+ remaining in incompletely washed ceria nanocubes increases the surface hydrophilicity. Sharp, low field resonances observed in spectra of non-calcined nanocubes arise from kinetically trapped sub-surface –OH.

Introduction

Ceria is an important material in catalysis and has received much study.[1-7] Its redox ability [8,9] and facile oxygen migration [10-16] are two of the properties of this metal oxide that are important in the mechanistic role of ceria as it is used in CO oxidation,[17-20] the water-gas shift reaction [21-25] and metal support catalysis. [3,26-29] Recently it has been found that ceria nanocrystals can be grown in different crystal morphologies with specific crystallographic planes presented on the crystal faces. Depending on synthesis conditions, particles with octahedral or cubic morphologies can be obtained, as can other shapes. [11,20,30] Nanoshaped ceria particles provide a well-positioned bridge that allows researchers to span the materials and pressure gap between low-surface area, well-defined crystallographic surface planes used in high vacuum surface techniques and high surface area, amorphous or ill-defined microcrystalline powders that can be studied under ambient or process conditions. The combination of high surface area and well-defined crystal planes on the nanoshaped particles makes them excellent platforms for studies of surface-dependent reactions by spectroscopic methods that require μ-mole or higher concentrations of surface species for adequate sensitivity.

Water adsorption and the nature of resulting hydroxyl groups on CeO_2 surfaces has been the subject of many studies both on single crystal surfaces and on high surface area materials. Interest is driven in part by the role of surface hydroxyls in promoting reduction of the ceria or as a probe of surface reduction and also in part due to interest in ceria

catalyzed water gas shift reaction. As reviewed by Mullins [7] there is evidence from both computational studies [31,32] and single crystal experiments [24, 33, 34, 35] that water may adsorb in both molecular and dissociated states on CeO_2. The extent/reversibility of dissociation and the relative stability of dissociated vs molecular states depend upon the coverage, presence of oxygen vacancies and the structure (coordination) of the surface. It has been proposed that adsorbed water may not fully dissociate but may be stabilized as hydroxyl pairs. [31] It seems likely that reversible dissociation/recombination may occur readily on CeO_2 in the unreduced state. In agreement with TPD and XPS experiments, calculations show that oxygen vacancies strengthen the binding energy of water and act as sites for water dissociation yet stabilize the dissociated fragments. [32, 36] Hydrogen bond interactions between water and CeO_2 becomes more favorable upon the introduction of oxygen vacancies on the surface. [36, 37] Hydroxyls resulting from water adsorption have been characterized by IR spectroscopy on high surface area CeO_2 [38] and single, double and triple coordinative bonding is observed. Coverage dependent studies indicate that interactions may change as water coverage increases. All of these results relate primarily to interaction of water with the clean or low coverage hydroxylated surface. Less is understood about the details of the interactions of water on the fully hydroxylated surface. Work by Herman et. al. [35] has suggested that the fully hydroxylated CeO_2(100) surfaces behaves as though it is hydrophobic. Comparison of water dissociation and desorption from dry and wet CeO_2 has been examined computationally. [32]

In this work ^{1}H Fast MAS NMR spectroscopy is applied to study the surface adsorption and dissociation of water on dry and hydroxylated cubic nanoshaped ceria. We show that the proton probe is insensitive to the redox properties of the ceria, providing a unique view of

the hydroxylated surface, not convoluted strongly by the electron-nuclear dipole-dipole interaction. The atomic concentration/integral area correspondence in ^{1}H NMR spectra is preserved. The spin counting experiments that establish this conclusion show that surface hydroxyls emanate from the full extent of the nanocube surface area. Surface –OH functionality and stability are defined in a direct way. The assignment and interpretation of these resonances as a function of temperature and pressure are the focus of this work. Computational methods were also used to analyze the water/ceria interactions. Since ceria cubes expose the {100} facet, a semi-infinite slab model of the (100) surface for ceria was used. While some consideration has been given to water adsorption on the (111) surface [31, 39-42] less work has been done on the (100) surface, [32] reporting lowest energy water structures on the ceria surface. The focus of the present work is on hydrogen-bond interactions to lattice oxygen that are relevant to the interpretation of ^{1}H NMR spectra of nanocube surface species and the energetic requirements of water dissociation.

Experimental

NMR. Solid-state MAS and fast MAS NMR measurements were collected on a Varian DD2 spectrometer using VnmrJ 3.2A software, a 16.4 T narrow bore magnet operating at a ^{1}H Larmor frequency of 700 MHz, and a 1.2 mm Chemagnetics-design Varian ultra-fast MAS probe. Measurements were taken using a standard one-pulse experiment with a typical $\pi/2$ pulse width of 3.6 μs, or a widely employed background suppression sequence (DEPTH, VnmrJ pulse sequence 'onepuldpth'). The onepuldpth sequence uses a single $\pi/2$ pulse followed by two consecutive windowless π pulses to discriminate against background signals. Chemical shifts were referenced with respect to external H_2O (δ = 0 ppm) using the adamantane resonance peak as a secondary reference standard (δ = 1.78

ppm). Consistent probe tuning was maintained by measuring the reflected pulse power using an oscilloscope, and adjusting the impedance match at the resonance frequency for < 1% reflected voltage, i.e., VSWR ≤ 1.02. Except for explicit variable MAS speed studies MAS rates of 20 and 40 kHz were routinely used.

Spin counting. Quantitative measurements of proton concentration on ceria nanoshapes were performed using adamantane as a spin-counting standard. Measurements were conducted using a new design end cap that incorporates a chamber permanently filled with adamantane. The adamantane-packed cap (adamcap) is used in place of the standard rotor end cap. A schematic of the rotor assembly is shown in Figure 1. Construction details are given in Figure S1.

Figure 1. Schematic representation of the rotor assembly with the adamantane-packed cap (adamcap) used in quantitative coverage assessments of ceria nanocubes.

The adamcap design addresses several experimental challenges: (1) the low proton density of surface species on these ceria samples (as low as 10^{-7} moles in this work) make it difficult to weigh the microgram amounts of adamantane needed to achieve peak intensities comparable to surface species; (2) correct relative signal intensity between the standard and sample is dependent on uniform distribution in the rotor, a condition difficult to achieve on small scale experiments where the sample is limiting; (3) the design provides

an efficient way to maintain a spin-counting standard from sample to sample; (4) Using standard glove box techniques for the removal and insertion of the rotor end cap and drive tip in an inert atmosphere provides the ability to perform physical and chemical manipulations on the sample in the packed rotor on the vacuum line. This procedure worked well on the ceria samples since once packed in the rotor and spun, the sample remained in the open-ended rotor sleeve under evacuation, heating and transfer conditions; (5) the separation of the sample and reference avoids chemical interaction with the sample and permits significant latitude in the choice of intensity standard.

The adamcap design maintains a fixed concentration and position of adamantane , hence, ^{1}H signal intensity, but since the sample and reference do not exist uniformly in the same volume element of the rotor, the 'effective' adamantane concentration must be calibrated in separate experiments. A weighed amount of benzoic acid-d_5, typically 1.4 mg, 11 μmol, packed in the rotor served as the proton concentration standard for the adamantane calibration, typically yielding an effective concentration of 22 nmol adamantane = 352 nmol H. The calibration experiments were performed using a single 90° pulse, preceded by two dummy pulses, and a 480 s recycle delay. The long delay is necessitated by the spin lattice relaxation time, T_1, of the acid proton of benzoic acid-d_5 (110 s). Spin counting experiments on the cerias used a constant recycle delay (40 s) since this choice allowed one background spectrum to be defined and used for the removal of the probe background signal from all ceria samples in the spin counting experiments.

Functional group concentrations on ceria were assessed from area ratios with respect to the effective H concentration of the adamantane reference. Peak areas were determined from one pulse or onepuldepth experiments. Both experiments give comparable

concentrations and validate the effectiveness of the background subtractions used throughout this work. Background signals were subtracted from all ceria spectra prior to spectral deconvolution to identify surface contributions from H_2O and –OH functionality (see Table 4). Proton concentrations on the ceria cube surfaces were measured on non-calcined and calcined cubes. Each of these cube samples underwent serial spin counting assessment in their 'as-received' state and twice more: after being heated in high vacuum for 2 h at 100 °C and then after being heated in high vacuum for 2 h at 400 °C. 'High vacuum' in this work refers to pressures less than 7.5×10^{-5} torr. One sample was examined at two additional temperatures, 160 and 200 °C (see Results). Proton concentrations are expressed as fractional surface area coverages, i.e., % monolayer (%ML), using the following specific areas for H_2O and –OH: 8.59 H_2O molecule/nm^2, the cross sectional area calculated from the spherical volume element of a water molecule; $2.99X10^{-23}$ cm^3/molecule); 13.6 OH/nm^2, derived from the fully hydroxylated ceria (100) surface. [24] A Brunauer–Emmett–Teller (BET) surface area of 17 m^2/g was used in the calculations for all ceria nanocube samples (see below).

Spin-lattice relaxation (T_1). T_1 measurements were performed using the inversion recovery experiment modified to include a DEPTH filter (Figure 2). Using background suppression in the T_1 data collection eliminates the dominant background for these low proton density cerias making the data analysis straightforward. For the inversion recovery pulse sequence, the π/2 and π pulses were 3.6 and 7.3 μs, respectively. A typical data set is shown in Figure S2.

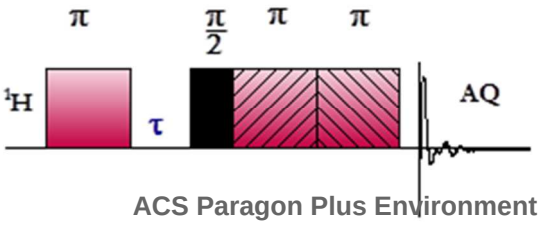

Figure 2. Inversion-recovery pulse sequence with DEPTH filter used to measure T_1 and efficiently suppress probe background signals.

Spin-spin relaxation (T_2). T_2 experiments were performed using a spin echo sequence: (π/2–τ–π–τ-acq.). Background T_2 spectra were collected over identical delay times and subtracted from the ceria sample spectra in "as-received" and 100 ˚C evacuated states prior to fitting intensities to a one- or two-component exponential decay function.

H_2O Addition Experiments. The controlled addition of water to a pre-dried sample was performed using calcined CeO_2 cubes. The cubes were heated under vacuum to 400 ˚C in a quartz reactor vessel for 2 h and allowed to cool to RT in vacuo. At room temperature the evacuated sample and a valved, evacuated frozen water reservoir were sealed off from the active vacuum to create an isolated system. As the water melted the sample was exposed to 4 increasing water vapor pressures. The sample was then sealed off from the water supply and allowed to take up water at each initial pressure for 1 hr.

Materials. For the nanoparticle synthesis all chemicals were handled in air and used as received. $Ce(NO_3)_3{\cdot}6H_2O$ (99%) was purchased from Sigma Aldrich. NaOH (≥ 97%) and constant boiling HNO_3 (68% HNO_3) were purchased from Fischer Scientific. NH_4OH (28-30%) and $Na_3PO_4{\cdot}12H_2O$ (98+%) were purchased from Acros Organics. Deionized water (18.2 MΩ) was used in all syntheses.

Synthesis of CeO_2 cubes. CeO_2 cubes were prepared based on a method published previously with some modifications.[43] Briefly, 0.434g $Ce(NO_3)_3 \cdot 6H_2O$ (0.001 mol) was dissolved in 2.5 mL H_2O. Then 4.8g NaOH (0.120 mol) was dissolved in 17.5mL H_2O and added to the $Ce(NO_3)_3$ solution. Upon the addition of NaOH solution, an opaque precipitate formed, indicating hydrolysis of $Ce(NO_3)_3$ and the formation of colloidal $Ce(OH)_3$. The solution was heated to 180°C for 24 hours, without stirring, in a 50 mL Teflon-lined stainless steel 4871 Parr reactor. The pressure reached ~7 bar. The resulting product was allowed to cool to room temperature, collected by centrifugation, dispersed in 10 mL ethanol and isolated via centrifugation. The product was then dispersed in 10 mL warm DI water and isolated via centrifugation. This washing procedure was repeated two more times. The product was dried under vacuum overnight at 100°C. The removal of Na impurities is important as previous studies have shown that alkali ion impurities can affect the reactivity of CeO_2-based catalysts.[44, 45] Na ion impurities were removed by dispersing the product in 2 mL of 0.1M NH_4OH, and suspending the mixture in an ultrasonic bath for two minutes at room temperature. The product was isolated via centrifugation, and washed 3 times in warm water. The product was then dispersed in 2 mL 0.1M HNO_3, and suspended in an ultrasonic bath for two minutes at room temperature. The product was isolated via centrifugation and washed again 3 times in warm water. The product was dried at 80 ±10 °C under vacuum (125 torr) overnight. CeO_2 cubes worked up by this procedure are labeled 'as-received non-calcined' cubes. In some samples the base and acid washing steps designed to remove excess Na^+ were omitted. These samples were labeled 'as-received, Na^+-contaminated' ceria nanocubes. Calcined samples were prepared by heating the as-received non-calcined cubes in air at 400° C for 4 hours, followed by cooling

to room temperature in air. Three-point BET analysis of N_2 adsorption isotherms was employed to obtain surface area measurements using a Micromeretics Gemini instrument. The calcined cubes have a surface area of 17 m^2/g.

Deuterated washes of CeO_2 nanoshapes. In separate experiments, as-received, non-calcined cubes were subjected to further washes with D_2O, ND_4OD/D_2O and $ND_4OD/D_2O/DNO_3/D_2O$. These washes were performed with deuterated reagents with > 99 atom % D as described below.

D_2O wash. The cubes were dispersed in 3 mL D_2O with sonication and isolated via centrifugation. This washing procedure was repeated two more times. The products were dried at 80 °C under vacuum (125 torr) overnight.

ND_4OD/D_2O wash. The cubes were dispersed in 2 mL 0.1M ND_4OD/D_2O with sonication and isolated via centrifugation. This washing procedure was followed by 3 D_2O washes (~3mL each). The cubes were dried at 80 °C under vacuum (125 torr) overnight.

ND_4OD/D_2O and DNO_3/D_2O wash. The cubes were dispersed in 2 mL 0.1M ND_4OD/D_2O with sonication and isolated via centrifugation. This washing procedure was followed by 3 D_2O washes (~3mL each). The cubes were then dispersed in 2 mL 0.1M DNO_3/D_2O (>99%) and isolated via centrifugation. This washing procedure was followed by 3 D_2O washes (~3mL each). The cubes were dried at 80 °C under vacuum (125 torr) overnight.

DFT Studies. Computational Details . All electronic structure calculations were carried out using the projector-augmented wave (PAW) method [46,47] as implemented in the Vienna ab initio simulation package (VASP).[48-51] Standard gradient-corrected exchange-correlation functionals are known to fail for the reduced ceria surface.[52] Therefore, the PBE+U [53,54]

functional within the DFT formalism was used consistently for all calculations. The commonly used value of 5 eV for U is optimized to position occupied Ce 4f states about 1.3 eV above the oxygen 2p states in bulk Ce_2O_3, [55] a value of 2-3 eV for U was suggested for the description of the redox chemistry over ceria [56] and bulk reduction energies [57] and a value of 2 eV was recommended for activation barriers.[58] In our work on methanol conversion over ceria [59] it was found for reduction processes that a value of 3.0 eV agrees better with hybrid functional results [60] than a value of 5.0 eV because of an increasing overstabilization of the reduced state with larger U. Here, a value of 3.0 eV for the effective U parameter was also chosen. This resulted in a lattice constant for CeO_2 of 5.46 Å. Spin-polarized functionals were employed with an energy cut off of 700 eV, and dipole corrections perpendicular to the surface. Dispersion corrections were included through the D3 method by Grimme. [61]

Following the experimental observation that the measured spectra are due to surface species and not due to populated defect or edge sites (see Coverage in Results section), a slab model with a vacuum layer of 15 Å was used. The (100) surface has a nonzero dipole moment normal to the surface. To avoid that dipole and consistent with experiment [62, 63] the oxygen terminated (100) surface was reconstructed by removing half of the oxygen atoms from the top of the slab leaving coordinative 'holes'. An equal amount of oxygen atoms was added to the bottom of the slab to conserve stoichiometry and, thereby, the oxidation state of Ce^{4+}. The oxygen atoms on both top and bottom form a checker board [c(2x2)] structure, which was found to be most stable.[64] The surface cell used included 9 atomic layers, where 6 layers were relaxed while the bottom 3 layers were fixed. For most calculations, one water molecule (associated or dissociated) was placed in the p(2x2) expansion of the surface cell corresponding to 1.7 water/nm^2. For the fully hydroxylated

surface, four dissociated water molecules were positioned within the p(2x2) cell. Minimum adsorbate structures were obtained by relaxation of the adsorbate and 6 surface layers. The minimum energy path was optimized with the nudged elastic band method (NEB) [65] where the tools provided by the Henkelman group [66] were used to set up the input. The path was represented by 13 images, which were optimized until the maximum atomic forces were below 0.05 eV/Å.

Results

^{1}H NMR spectra of ceria nanocubes: General characteristics. Cerias exposed to ambient temperature and humidity conditions of the laboratory (60% relative humidity) possess multiple layers of physisorbed water on their surfaces. The ^{1}H NMR spectra of a commercial ceria (uncharacterized morphology) and of ceria cubes in as-received non-calcined condition are dominated by a resonance at 6±1 ppm, with a concentration-dependent chemical shift (Figure 3). This peak arises from loosely held physisorbed water as indicated by the fact that it is eliminated by vacuum evacuation at room temperature or under mild heating.[67] Additional weak proton resonances appear on the shoulders of the dominant water resonance. The number and type of these peaks differ between the commercial and the cubic cerias, and arise from H_2O or -OH species residing at specific crystal sites.

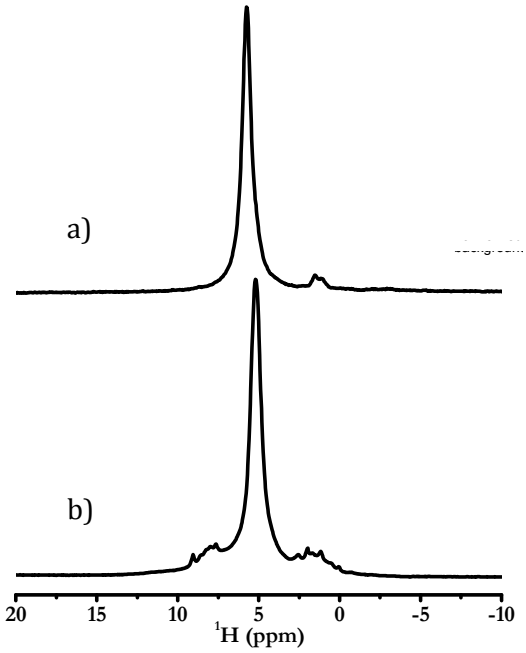

Figure 3. ^{1}H MAS NMR spectra of a commercial (a) and nanocube (b) ceria. Each material has physisorbed water sufficient to form several monolayers coverage.

Exemplary hydroxyl and water resonances from ceria sites are shown in Figure 4a-c, for an as-received, non-calcined nanocube sample evacuated at sequentially higher temperatures. The plot above the spectra (Fig. 4d) depicts the decrease in hydroxyl (-OH) (green line) and water (blue line) concentration derived from five spectra sampled over the 25-200 °C temperature range. The proton resonance from physisorbed water (6±1 ppm, Fig.4a) represents 0.9 ML and drops precipitously at room temperature to 0.1 ML by application of high vacuum (<7.5 X10^{-5} torr). The initial water concentration in as-received samples may be 2 or more ML depending on the sample history (see Figure 3). More than 90% of the water is removed from the sample by the application of high vacuum at RT. With the loss

of loosely held water, good resolution is observed between the remaining high field (ca 1ppm) and low field (ca. 9 ppm) bands, both due primarily to hydroxyl. A possible exception is the shoulder peak evident at ca. 3 ppm in Figure 4b (arrow) recorded after heating the sample to 100 °C for 2 h. A cluster of peaks centered at 3 ppm due to water is prominent in samples contaminated with Na^+ (see below), suggesting that the shoulder peak in Figure 4b could be due to water associated with this alkali impurity. Residual physisorbed water is removed from the sample after the cubes are heated to 200 °C (Figure 4c). The hydroxyl band intensities, 0.9 ML at RT and 1 atm, decrease to 0.7 ML under high vacuum, and decrease further to 0.5 ML at 200 °C (Figure 4c, d). Finally, evacuation at 400 °C removes essentially all protic species from the ceria surface (not shown).

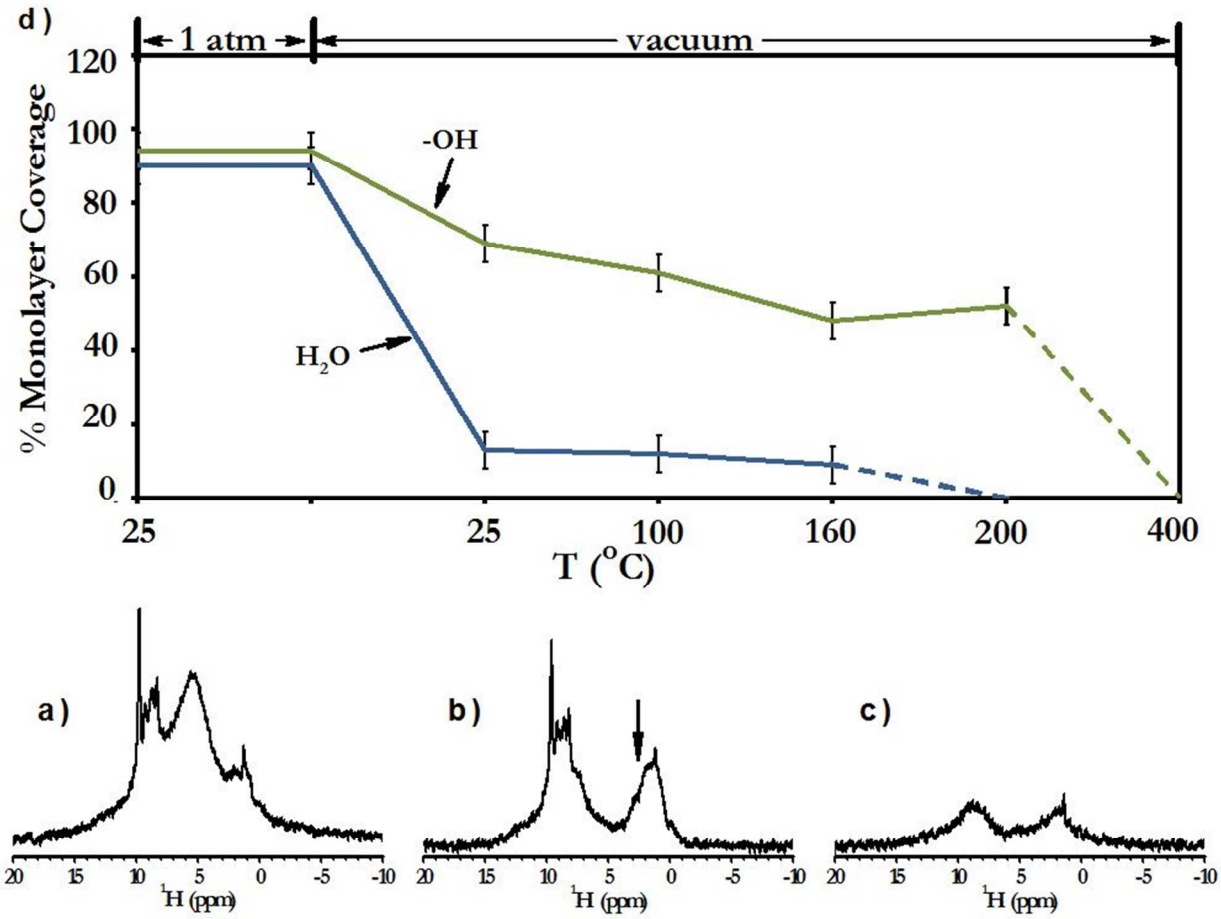

Figure 4. ^{1}H MAS NMR spectra of non-calcined cubes showing pressure and temperature response of the integrated intensity of water and –OH resonances: a. as received, non-calcined cubes (previously dried at 80 ±10 °C under mild vacuum, 125 torr, overnight: see Experimental section). This spectrum was recorded at 25 °C; b. The spectrum of the same sample after heating at 100 °C for 2 h under high vacuum; c. the spectrum of the same sample after heating at 200 °C for 2 h under high vacuum. d. The plot displays percent monolayer coverage of –OH (green line) and physisorbed water (blue line). The ordinate scale is derived from spin counting experiments (Table 1).

Superimposed upon the low field band are a group of four sharp resonances between 8 and 10 ppm, prominent in Figure 4a, b. After heating to 200 °C under high vacuum, the broad low and high field bands decrease and the four sharp resonances vanish (Figure 4c). The intensity of these bands are depicted with finer temperature resolution in Figure 5, where it is evident that the 8-10 ppm resonances are eliminated from the spectra by heating the sample to 160 °C. Also, the problematic 3 ppm shoulder peak seen in Figure 4b is eliminated by heating the sample to 120 °C.

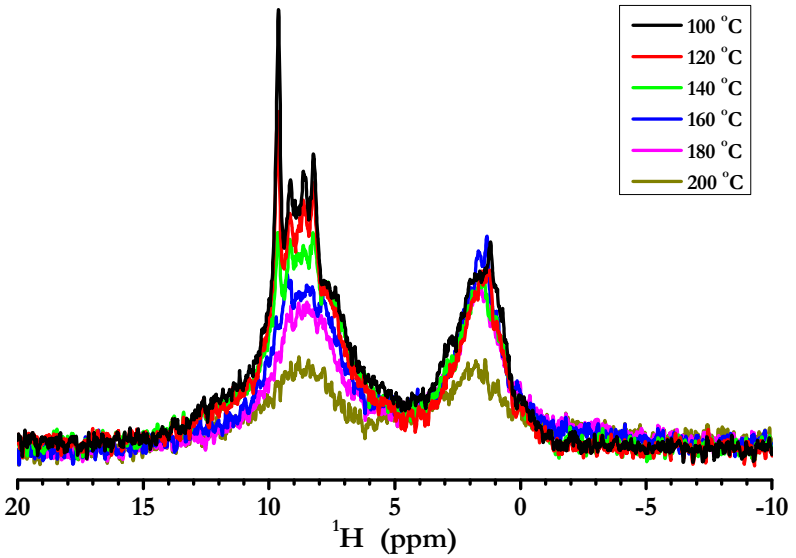

Figure 5. ^{1}H MAS NMR spectra of non-calcined nanocubes exposed to two hour high vacuum cycles at temperatures between 100 and 200 °C. Residual water leaves in this interval and the -OH concentration slowly decreases.

Sodium ions on nanocube surfaces alter surface wettability. The appearance of ^{1}H MAS spectra of cubes depends on the details of the preparation as well as the extent of retained water. Figure 6a shows the spectra of non-calcined, Na^{+} contaminated cubes, the result of omitting the base-and acid washing steps following the cube synthesis. The presence of potassium has been shown to impact catalytic activity of ceria-based catalysts.[44, 45] Presumably, sodium will elicit a similar behavior. Figure 6b and c show spectra of these cubes after water washes to different extents. In Figure 6a at least 11 unique resonances spanning the 1-10 ppm chemical shift range are observable, including a very intense peak at 3ppm. The resolved clusters of resonances in the 1.5-4 ppm region are only observed in ceria cube samples with Na^{+} contamination.

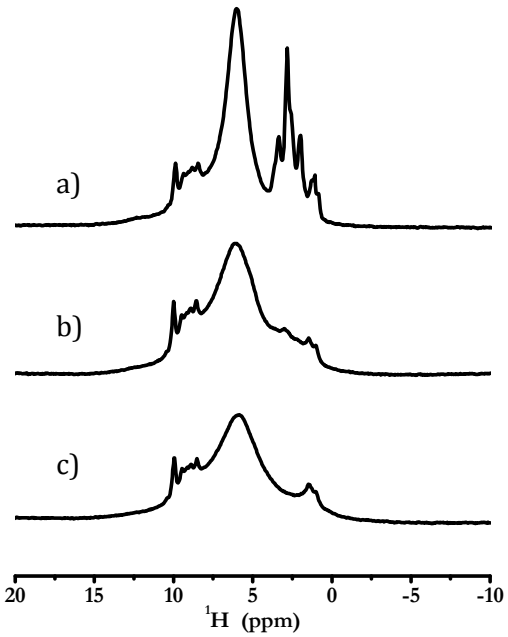

Figure 6. ^{1}H NMR spectra of ceria nanocubes; (a) as received, Na^{+}-contaminated (b) the same sample further washed with H_2O, and (c) the same sample washed with D_2O four times followed by an H_2O wash. These nanocubes contain a sodium ion contaminant that appears necessary for the observation of the sharp upfield resonances assigned to molecular water (3 ppm cluster).

The spectra in Figure 6 a-c are arranged in order of increasing half-height linewidth of the physisorbed water resonance at ca. 6 ppm. The sharp resonances in the 1.5-4 ppm region (3 ppm peak maximum) in Figure 6a appear to broaden in concert with an increase in the linewidth of the physisorbed water resonance. This parallel broadening is consistent with an exchange process occurring between the protons of the 1.5-4 ppm sites and physisorbed water. In the high temperature limit of a classical two-site exchange process, the resonance appears at the weighted average of the separate resonances. This criterion does not strictly apply in the present case since the samples in Fig. 6 have separate washing histories and there is no expectation that the concentration of the two populations remain the same over the suite of samples. We suggest that the sharp resonances arise from molecular water or water clusters associated with CeO-Na+ sites. The exchange is postulated to occur between these water clusters and bulk physisorbed water. In effect, the polar $CeO^{-}Na^{+}$ on the surface enhances the interaction between the surface and physisorbed water, locally increasing the hydrophilicity at these sites relative to alkali-free ceria. In contrast, the 9 ppm resonance band and the sharp 8-10 ppm resonances are impervious to changes in water concentration and show no indication of participation in dynamic exchange processes.

All ceria cube spectra in Figure 6 contain a weak signal at 1.2 ppm, often occurring with a companion peak at 0.8 ppm. Resonances at these chemical shifts have been assigned to –OH on the ceria (111) surface.[68, a] The resonances are not involved in exchange broadening processes under the observation conditions. The (111) surface occurs on imperfect cubes as a truncated surface normal to the cube diagonal at the confluence of beveled edges.[69] The low concentration of these resonances in the cube spectra is consistent with this assignment.

---

[a] (Footnote): Our chemical shifts differ from those reported by Lyons et. al. by a common offset of +2.4 ppm. [68] The –OH chemical shift on octahedral ceria reported therein (-1.2 ppm) appears at +1.2 ppm in the present work, relative to the adamantane reference at δ1.78 ppm. We have confirmed the difference arises from a referencing error by direct synthesis of EVAP600 described by Lyons et. al. [68], for which we find a +1.2 ppm chemical shift for the resonance assigned to surface –OH on the ceria (111) surface.

Effects of calcination. Since CeO_2 catalysts are usually calcined prior to use, we probed the effects of high temperature oxidation on the as-received, non-calcined cubes. Some of these samples were calcined in air at 400 °C for 4 h followed by cooling, either in laboratory air or after prompt transfer to vacuum. Cooling in vacuum results in a null spectrum where only the background signal from the probe is observed, indicating that all protic species have been removed. Cooling the sample in laboratory air instead leads to the

^{1}H NMR spectra shown in Fig 7b. The needle-like 8-10 ppm resonances ($\nu_{1/2}$ = 0.3 ± 0.1 ppm) that are seen in the spectra of as-received, non-calcined cubes (Figure 7a) do not appear in the air-cooled calcined cubes. As shown in Fig 5 these needle-like resonances can be removed under mild conditions, i.e., heating in vacuum at 160 °C. The functionality that yields these resonances does not recur upon re-exposure of the calcined sample to air. Nor do the resonances recur in non-calcined samples once they are removed by mild heating. Multiple attempts to reintroduce the resonances by exposure of the cubes to liquid water or water vapor between room temperature and 160 °C proved unsuccessful.

Apart from the sharp peaks, heterogeneous distributions of local sites result in broadened resonance bands ($\nu_{1/2}$ = 2-5 ppm) that typify both non-calcined and calcined cube spectra. The structure inherent in the low field resonance bands, extending to ca. 12 ppm, presents strong evidence for multiple hydrogen-bonded sites. With allowance for the different extent of residual water, a close correspondence between non-calcined (Figure 7a) and calcined (Figure 7b) spectra of cubes is observed.

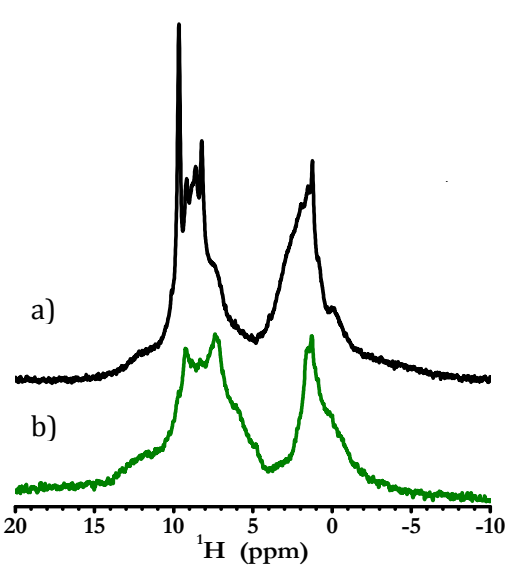

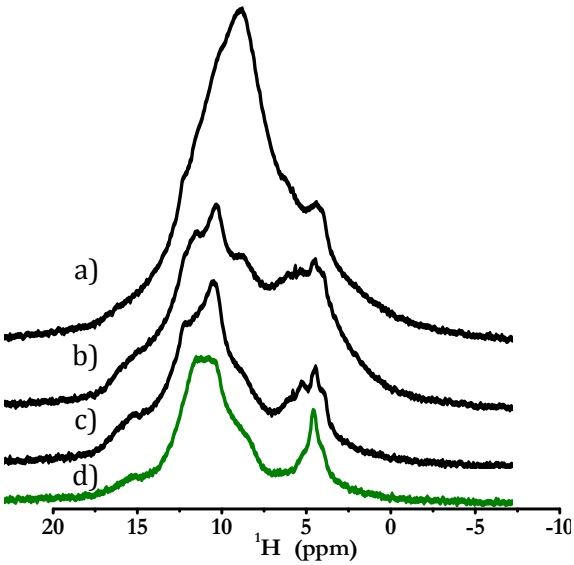

Figure 7 (left). ^{1}H MAS spectra of non-calcined and calcined ceria nanocubes: a. synthesized and then dried at 80 ±10 °C under weak vacuum (125 torr) overnight. b. same as a, then calcined at 400 °C, 4 h, cooled in air, and dried at 100 °C under vacuum. The cerias retain different extents of physisorbed water (peak centered at 7 ppm).

Figure 8 (right). ^{1}H MAS NMR spectra of dry ceria nanocube re-exposed to water. The sample was heated to 400 °C in high vacuum to remove all protic surface functionality, cooled in vacuum, and then exposed to water vapor at: (d) 10 mTorr; (c) 200 mTorr: (b) 500 mTorr; (a) 950 mTorr, respectively.

H_2O Addition. The controlled addition of water to dry CeO_2 cubes was studied. The dry sample, free of proton functional groups, was prepared by heating the calcined cubes under

vacuum to 400 ˚C in a quartz reactor vessel for 2 h and cooling to RT under vacuum. The dry sample was exposed to water vapor at four increasing pressures for 1 h at each pressure. The spectra obtained at each pressure are shown in Figure 8. Water uptake increases with pressure and, at the lowest pressure, the appearance of both 1 ppm and 9 ppm bands appear fully populated. After the first dose (Figure 8d) the accruing area is largely due to the emergence of a broad physisorbed water resonance, not to a specific increase in the 1 ppm or 9 ppm resonance bands. Note the similarity between Figure 8d and the spectrum generated by drying as-received non-calcined cubes at 100 °C under vacuum, Figure 7b. The hydrogen-bonded –OH band at 9 ppm is dominant in both samples but the relative population of the 9 and 1 ppm bands show some variation dependent on the sample preparation. This may be ascribed to differential surface annealing effects which alter the extent of hydrogen-bonding among the surface –OH, as discussed in the DFT calculations below. The initial exposure of a dry, pristine (100) surface to water results in the immediate formation of hydroxylic species, i.e., adsorption and water dissociation occurs simultaneously on this surface.

Attempted Deuteration of Ceria Cubes. Washing ceria cubes with deuterated aqueous acid and base solutions was explored as a potential technique to discriminate among surface sites based on their ease of exchange. Figure 9 compares the spectrum of as-received non-calcined cubes (Fig. 9d) with the spectra obtained after washing in D_2O (Fig. 9c), ND_4OD/D_2O (Fig. 9b), and DNO_3/D_2O followed ND_4OD/D_2O (Fig. 9a), as described in the Experimental Section. Unexpectedly, the exchange of surface hydroxyls does not occur under the washing conditions, causing insignificant change in the integrated area of the surface signals. Under these conditions, no surface –OH functionality participates in

H/D exchange. More severe conditions (sonication in D_2O at elevated temperature for hours) also failed to achieve exchange of surface –OH sites on ceria nanocube surfaces.

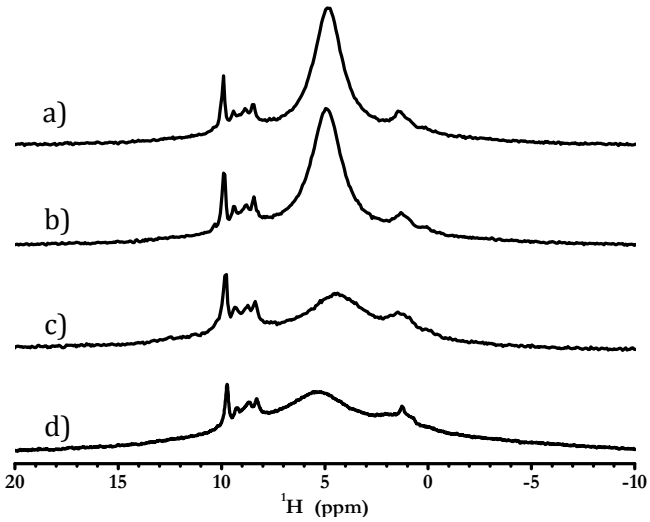

Figure 9. ^{1}H MAS NMR spectra of non-calcined cubes washed with a) deuterated acid, followed by deuterated base and D_2O; b) deuterated base and D_2O; c) D_2O; d) H_2O.

Coverage. Surface coverage estimates can be used to discern whether the surface functionality derives from point defects on the crystal surface or represent populations of functional groups that engage a significant fraction of the crystal surface. Dependent upon the value of surface coverage, the spin counting results may inform whether the electron-nuclear dipole interaction from unpaired electrons at Ce^{+3} sites is manifest in the ^{1}H fast MAS NMR spectra of ceria nanocubes. Coverage was estimated by spin counting using adamantane as an internal reference, measuring the area ratio of the surface signals against the reference area. The spin counting procedure is outlined in Figure S3-S7 and accompanying text. The coverage results for as-received non-calcined cubes in Table 1 show the decrease in surface concentration of both physisorbed water and surface

hydroxyls (-OH) as the sample temperature is increased under vacuum. The loss of hydroxyl functionality as the temperature is raised correlate well with data from other spectroscopic probes, notably solid-state ^{17}O NMR [70] and O1 XPS [24, 35] studies. The coverages in Table 1 are the basis for the ordinate scale in Figure 4d. The spin counting experiments demonstrate that –OH resonances occupy the available surface area of the as-received, non-calcined cubes (0.9 ± 0.2 ML). Monolayer definitions are based on 13.6 – OH/nm^2, the –OH density of a fully hydroxylated CeO_2 (100) plane [24] and 8.59 H_2O/nm^2. The latter value is the cross-sectional area of a H_2O molecule derived from the volume of one H_2O molecule, 2.99x10^{-13} cm^3, calculated from first principles (density and Avogadro's number). Multiple determinations from different samples of cubes yielded –OH surface coverages of 0.8 ±0.2 ML. This result is in agreement with the coverage determined for stoichiometric (100) surfaces by TPD measurements at low temperature (0.9 ML) [35] and with the prediction of DFT calculations presented below.

Table 1. % Monolayer coverage on non-calcined ceria nanocubes for water and hydroxyl as a function of pressure and temperature.

Treatment	H_2O (% Monolayer) [a]	-OH (% Monolayer) [b]	Total (% Monolayer)
25 °C, 1 atm.	90	94	184
25 °C, vacuum [c]	13	69	82
100 °C, vacuum	12	61	73
160 °C, vacuum	9	48	57

200 °C, vacuum	0	52	52
400 °C, vacuum	0	0	0

a. Water coverage (±20 %) based upon spin counting areas use the following monolayer definitions: 1ML = 8.59 H_2O molecule/nm^2 (based on cross sectional area of the spherical volume of a water molecule, 2.99 x 10^{23} cm^3/molecule). b. Hydroxyl coverage (±20 %): 1ML = 13.6 OH/nm^2, derived from the fully hydroxylated ceria (100) surface. [24] All calculations use a ceria nanocube surface area of 17 m^2/g. c. Pressure less than 7.5 x 10^{-5} torr.

Fast MAS ^{1}H NMR of Ceria Cubes. In crystalline hydrates, water of hydration can be fixed in the crystal and give rise to strong homonuclear dipole-dipole coupling between the intramolecular proton pair of the water molecule. The magnitude of the coupling is greater than observed for isolated, surface-bound hydroxyl groups. This effect has been used in silicate glasses to distinguish between H_2O and OH resonances based on the strength of the dipolar coupling, manifest in the line widths of static NMR spectra or in the relative intensity of the sideband/centerband area in ^{1}H MAS NMR spectra. The strong dipolar coupling of water hydrates result in static line widths on the order of 40 kHz and produces two strong sideband pairs possessing ca. 4 times the intensity of the centerband resonance in silicates at 10 kHz MAS speeds. Isolated hydroxyl resonances have static linewidths of 10 kHz and produce one weak pair of sidebands possessing < 0.2 times the centerband intensity at 10 kHz MAS speeds. [71]

^{1}H-^{1}H dipole strength is assessed for ceria spectra in Figure 10 which displays wide sweep width, variable MAS ^{1}H NMR spectra of as-received non-calcined ceria cubes. The spectra are recorded with MAS speeds from 0 to 35 kHz. The spectra reveal two resonance bands at 1 and 9 ppm, that are well-resolved at the lowest MAS rate (10 kHz), with the needle-like 8-10 ppm resonances riding on the low field band. Centerband resolution does not improve at higher MAS speed. A comparison of the 15 kHz MAS spectra show that both the broad 1 and 9 ppm resonances have small first order side bands typical of hydroxyl groups. [71] They can not arise from fixed, hydrogen-bonded water. The sharp resonances at 8-10 ppm show no side band intensity, even at the lowest MAS speed. The sideband intensity trends seen in cubes are also observed in commercial ceria samples (see Figure S8).

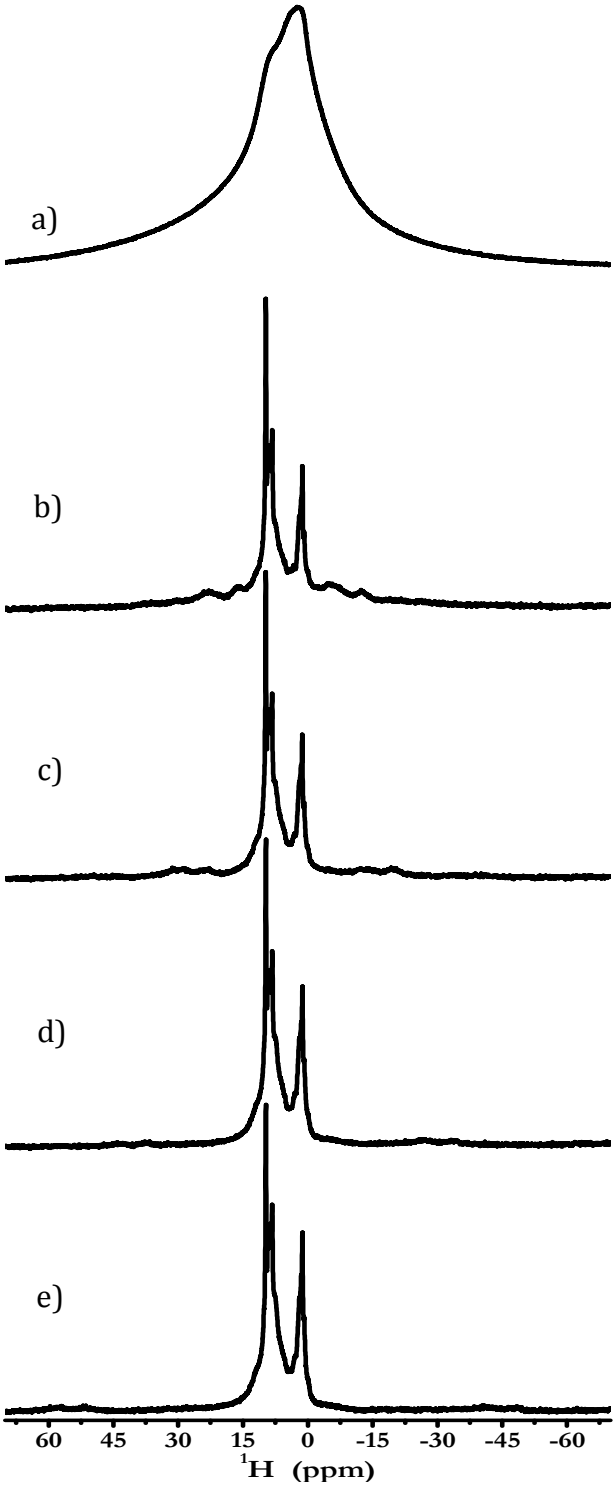

Figure 10. MAS dependence of the ^{1}H NMR spectra of non-calcined cubes, a) static, b) 10kHz, c) 15 kHz, d) 25 kHz, e) 35 kHz. The ratio of sideband to centerband area indicates weak ^{1}H-^{1}H dipolar coupling typical for isolated –OH functionality.

Spin-lattice relaxation, T_1. A summary of the spin lattice relaxation (T_1) data recorded at room temperature for ceria nanocubes in as-received, non-calcined (sample1), D_2O-washed (sample 2), and calcined (sample 3) states is reported in Table 2. T_1 data were measured first on a sample displaying a resonance for physisorbed water (labeled 'as-prepared' in Table 2) and were measured again after the sample was heated to 100 °C for 2 h under high vacuum. The relaxation time data span more than three orders of magnitude for the functionality monitored in the spectra. Except for the physisorbed water resonance, T_1 displays bimodal relaxation character.

The dominant physisorbed water resonance in 'as-prepared' samples, 5.5 ±0.1 ppm, has T_1 = 10 ms for all samples. T_1 from surface resonances of the cubes were monitored at peak maxima, near 1 ppm for the high field band, and around 9 ppm for the low fields band. All these resonances show one T_1 component equal to that of physisorbed water. The second component displays a longer T_1, 100s of ms for the 1 ppm band and several seconds for the 9 ppm band. No physisorbed water resonance is apparent in the spectra of samples dried at 100 °C. In comparison to the as-prepared samples, the shorter T_1 component of the 1 and 9 ppm bands increases to 100s of ms while the long T_1 component remains unchanged.

The constant value of the long T_1 component upon removal of physisorbed water indicates that the spin systems for the physisorbed water and for the surface species are isolated from each other, i.e., no cross-relaxation occurs between spin populations. This remarkable observation is affirmed by the invariant T_1 of the 'as-prepared' samples that have been washed with D_2O (sample 2) or calcined (sample 3). Both of these procedures would be expected to reduce the strength of the ^1H-^1H dipolar interaction in the affected spin populations and lengthen the T_1 of the surface -OH functionality if they were in

intimate contact. The relaxation trends are prima facie evidence for the isolation of the physisorbed water and surface hydroxyl spin systems, and consequently the isolation of the molecular species.

The T_1 of the needle-like resonances are the same as the underlying broader resonance bands. This follows from the bimodal analysis of as-received non-calcined nanocubes and from T_1 comparison of the as-received,yn non-calcined, and calcined samples.

Spin-spin relaxation, T_2. A summary of T_2 values for non-calcined cubes is given in Table 3. T_2 values for as-received non-calcined cubes are compared with those from a sample dried under vacuum at 100 °C. The data require a two-component fit. The short component in both samples is on the order of 100 μs, the T_2 of the physisorbed water resonance. The resonances of hydroxyl sites are on the order of ms, one to two orders of magnitude longer than the water T_2. To a first approximation, the long T_2 is independent of the water concentration suggesting that the surface sites are not in intimate contact with the physisorbed water component. The four T_2 values of the sharp 8-10 ppm resonances differ significantly from each other, indicating that these protons are reflecting unique environments. The long T_2 of the surface –OH resonances is good evidence that excludes the assignment of these resonances to -OH hydrogen-bonded to water. Such species on the surface of silicas show T_2 on the order of 50 μs, resulting from the close proximity of the –OH and H_2O protons. [67]

Table 2. Spin-lattice relaxation (T_1) data summary for as-received, D_2O washed and calcined cubes (2 component fits).

	As-prepared				Dried at 100 °C in vacuum		
	δ (ppm)	T_1 (ms)	T_1 (s)		δ (ppm)	T_1 (ms)	T_1 (s)
1. Sample 1, (as-received, non-calcined)	1.23	10	0.43		1.28	100	0.46
	5.44	10					
	8.21	10	3.2		8.23	150	3.2
	8.57	10	4.0		8.59	190	4.0
	9.16	10	3.1		9.15	480	3.0
	9.65	10	5.1		9.65	560	5.8
2. Sample 2, (D_2O-washed)	1.23	10	0.43		1.28	460[a]	0.46[a]
	5.40	10					
	8.21	10	2.9		8.23	150	3.1
	8.57	10	3.8		8.59	190	4.3

	9.16	10	3.1		9.15	460	3.0
	9.65	10	5.2		9.65	560	4.6
3. Sample 3, (calcined)	1.24	100[b]	100[b]		1.24	80	0.63
	5.59	10					
	9.10[c]	30	4.3		9.10	100	3.8

a. b. Data fit best to a single exponential. c. The reported T_1 is the average value of measurements taken at 8.65 and 9.50 ppm, local peak maxima in this region. T_1 monitored at 12 ppm, i.e., along the broad low field tail of the downfield resonance band, is 4±1 s.

Table 3. T_2 data summary for as-received and vacuum-dried (100°C) non-calcined ceria nanocubes (2-component fit)

As-received				Dried at 100 °C in vacuum		
δ (ppm)	T_2 (ms)	T_2 (ms)		δ (ppm)	T_2 (ms)	T_2 (ms)
1.23	0.1	1.1		1.23	0.1	0.7
5.64	0.1					
8.21	0.8	4.7		8.21	0.1	3.5

8.60	0.5	2.1		8.57	0.1	1.3
9.16	0.7	8.0		9.16	0.1	4.7
9.65	2.1	30.6		9.65	0.1	9.9

DFT studies. Water was found to adsorb on the (100) surface in the coordinative 'holes' (described in Experimental). Geometry optimizations, where the water molecule was initially placed in an atop position above cerium converged to structures with water adsorbed in a hole. We found multiple structures distinguished by the orientation of water and enabling hydrogen bonding at varying strengths. Figure 11 shows three exemplary water structures with (a) zero, (b) one, and (c) two oxygen-hydrogen distances below 2 Å. Figure 11 also includes the adsorption energies calculated as

$$E_{ads} = E_{surf} + E_{water} - E_{surf/water}, \quad (1)$$

where E_{surf} is the energy of the clean surface, E_{water} is the energy of the isolated water molecule, and $E_{surf/water}$ is the energy of water adsorbed on the surface. A positive adsorption energy indicates exothermic adsorption. Consistent with prior work [32] the adsorption energy of water is about 1 eV. The adsorption energies of the water structures shown in Figure 11 (a)-(c) are within a narrow energy range (0.94 – 1.09 eV) indicating that hydrogen bonding between the water molecule and surface oxygen has a minor effect on the stability of the water/ceria system.

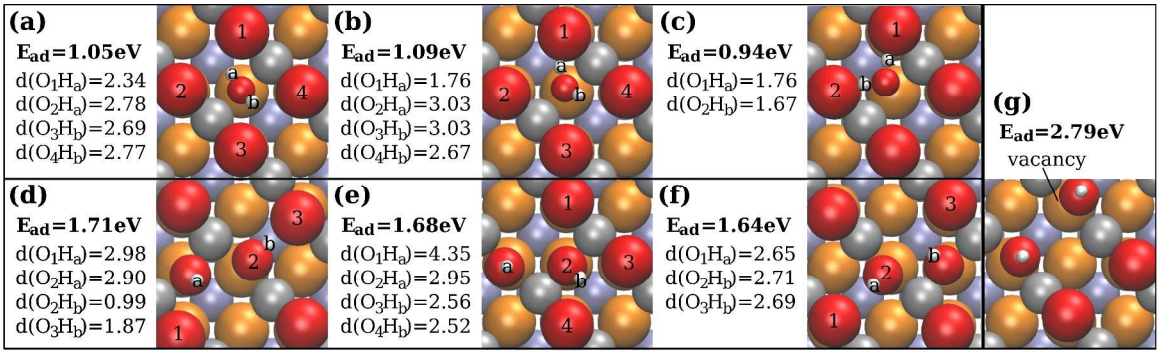

Figure 11. Top view of water (a) – (c) and dissociated water (d) – (f) on the oxidized (100) ceria surface, and of dissociated water (g) on the partially reduced (100) ceria surface; crystal radii [73] used for rendering of the surface, covalent radii [74] for adsorbates except hydroxyl oxygen, for which an average of crystal and covalent radius was used; orange – oxygen, red – oxygen top layer and adsorbates, white – hydrogen, purple – cerium, silver – cerium second layer; distances in Å.

When one of the O-H bonds is cleaved, a hydroxyl is formed that is located in the hole position (hole hydroxyl) while the hydrogen atom forms a second hydroxyl with a lattice oxygen (surface hydroxyl). There is a slight distinction between the hydroxyls due to the difference of the coordination sphere in the two positions. While the surface hydroxyl is surrounded by next nearest neighbor oxygen atoms, the hole hydroxyl is enclosed by nearest neighbor oxygen atoms with next nearest neighbor positions empty. Two of the next nearest neighbor surface oxygen atoms are available (not blocked by second row cerium atoms) for strong hydrogen bonding when the surface hydroxyl rotates such that the hydrogen atom is integrated in the top layer, see Figure 11 (d). Again, we find a variety

of structures that are distinct by the orientation of the hydroxyls; three examples are shown in Figure 11 (d)-(f). Selected oxygen/hydrogen distances and dissociative adsorption energies are also reported in Figure 11, where $E_{surf/water}$ is the energy of dissociated water on the ceria surface in Eq. (1) for structures (d)-(f). Similar to the associated water systems, the dissociative adsorption energies for the hydroxyl structures shown in Figure 11 are nearly equal (1.64 to 1.71 eV) and consistent with the value given in prior work.[32]

Figure 12 depicts the NEB path for the cleavage of one of the oxygen/hydrogen bonds in water in the energetically lowest structure given in Figure 11(b). The path does not reveal a barrier for dissociation suggesting that adsorbed water is a meta-stable state on a flat potential energy surface. This is in agreement with the experimental finding that dissociation occurs immediately upon water exposure. Depending on the orientation of the resulting hydroxyls on the cube surface, hydrogen bonds of different strength are formed between hydroxyl H and lattice O explaining different chemical shifts in the NMR experiments. Since these structures are energetically very close, we expect that they are populated to a similar extent, contributing to the broadening of the experimentally observed NMR peaks.

The partially reduced surface is modeled by removing one surface oxygen resulting in an oxygen vacancy with two electrons remaining in the surface. These electrons localize in cerium 4f-bands reducing two Ce^{4+} to Ce^{3+} ions and were reported to be located next to the vacancy in the lowest energy solution.[72] However, with our computational setup (different DFT functional and surface cell expansion), an energetically lower solution is obtained

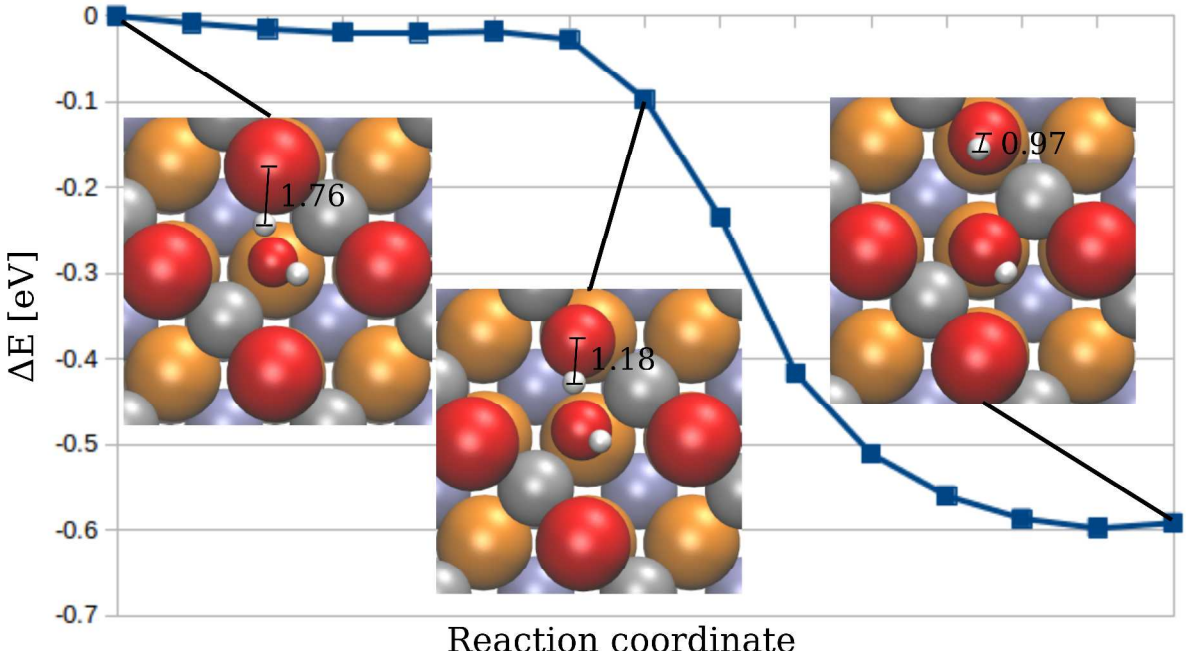

Figure 12. Energy difference as a function of the reaction coordinate for the O-H bond. Data points corresponds to NEB images; radii and coloring as in Figure 11; distances in Å.

when the Ce^{3+} ions are located nearest and next nearest to the vacancy in the second layer. This is the Ce^{3+} configuration we use in our calculations, although, we have not searched for a globally lowest solution. When we place water as initial structure either in the vacancy or in the hole position, geometry optimizations converge to a solution where water is dissociated. Although an undissociated structure has been reported previously,[32] it is unlikely that this structure is a minimum on the potential energy surface corresponding to the computational parameters used herein. According to our results, regardless of the degree of surface reduction, water is expected to undergo spontaneous oxygen/hydrogen bond cleavage on the (100) surface.

When water undergoes O-H bond cleavage in the presence of a vacancy, the hydroxyl occupies the vacancy and the hydrogen is located on a neighboring surface oxygen. The resulting structure is shown in Figure 11(g). Geometry optimizations with hydroxyl occupying the hole position as the initial structure converge to a structure where hydroxyl is situated in the vacancy. Without an adjacent hole position occupied by hydroxyl, the hydroxyl(s) in Figure 11(g) prefer to orient normal to the surface. At the 3.4 OH/nm^2 coverage (0.25 ML) used in the calculations, energetically close structures with tilted hydroxyls are not observed. Hydroxyls in Figure 11 (g) are next nearest neighbors, each surrounded by empty hole positions. Due to periodic boundary conditions and limited cell size, there are no oxygen atoms available to share a hydrogen atom as observed in structure Figure 11(d) on the oxidized surface. Each hydroxyl has either another hydroxyl or an oxygen blocked by a second row cerium atom (shown in gray in Figure 11) as a neighbor. To model a hydroxyl arrangement that is not artificially limited by periodic boundary condition and allows for strong hydrogen bonding to a surface oxygen, we use as initial structure a configuration, where the hydroxyls are second nearest neighbors. We then rotate one or both hydroxyls towards the surface for hydrogen to interact with an available surface oxygen. Geometry optimizations lead again to a structure where the hydroxyls are standing up. It appears that the hydroxyl orientation parallel to the surface does not correspond to a minimum structure when hydroxyl occupies the vacancy position. The dissociative adsorption energy (defined as above but with the surface containing a vacancy) is included in Figure 11(g) and is similar to the adsorption energy reported by Molinari.[32] At the same coverage of 3.4 OH/nm^2, implying a more spacious oxygen top layer in the vacancy structure, water binds dissociatively, about 1 eV more strongly over a

vacancy than on the oxidized (100) surface. Note, that although the vacancy appears to be healed by hydroxyl, the surface remains reduced with two Ce^{3+} ions occupying nearest and next nearest neighbor positions relative to the vacancy.

The experimental finding that the fully hydroxylated surface does not interact with water was examined computationally. The hydroxylated surface has a large number of minimum structures that are distinguished by the orientation of the hydroxyls to each other. Many of these are accessible at the experimental conditions and the exploration of each configuration is beyond the scope of this work. Instead, a two-stage approach was employed, where six configurations of a water molecule with the hydroxylated surface were first created and then the energy for water removal for each sample configuration was measured. This approach allows for nominal alteration of the minimum structures of the hydroxyls that are not engaged in water interactions during re-optimization of the water-free hydroxylated surface. We obtain a representative range of values for the local interactions between water and the hydroxylated surface that we compare to the interaction of water with itself.

The binding energy of a water molecule within a water network was estimated from a water cluster consisting of five water molecules. The center water molecule is connected through hydrogen bonds with four surrounding water molecules. The binding energy per water molecule is estimated as

$$E_{bind} = E_{4w} + E_{1w} - E_{5w}, \qquad (2)$$

where E_{5w} is the energy of the optimized water cluster, E_{4w} is the energy of the cluster, where the center water molecule is removed, and E_{1w} is the energy of an isolated water molecule. A value of 0.92 eV for this energy was calculated.

To estimate the interaction energy of a water molecule with the hydroxylated surface, the fully hydroxylated surface is constructed orienting half of the hydroxyls normal to the surface and half tilted towards the surface, as in Figure 13 (a). This corresponds to the structure shown in Figure 11(e) periodically repeated and using a p(1x1) cell. The high coverage reduces the dissociative adsorption energy per water from 1.68 eV to 1.33 eV. Note, the so generated fully hydroxylated surface is not necessarily the energetically most favorable. A water molecule is then added to the surface resulting in six structures that are distinguished by the orientation of the water molecules. All optimizations of the water/hydroxyl aggregates lead to similar geometries where at least two hydroxyl hydrogens interact with water oxygen and one of the water hydrogens interacts with an oxygen of an hydroxyl that is tilted toward the surface. An exemplary structure is depicted in Figure 13(b). The adsorption energies for water on the initial hydroxylated surface are 0.73-1.54 eV These, however, include energy differences due to the response of hydroxyls that do not interact with water. To obtain water adsorption energies that estimate only water hydroxyl interactions, the water molecule was removed and the hydroxylated surface was relaxed. For the configuration shown in Figure 13(b), the water adsorption energy relative to the relaxed surface shown in Figure 13(c) is 0.04 eV. For all six exemplary calculations, the hydroxyls on the surface previously engaged with water reorient to interact better with each other. The adsorption energies, obtained by letting the surface respond to water removal, range from 0.00 – 0.78 eV. This suggests that water may indeed prefer to participate in the hydrogen-bonded network with other water molecules (compare to the binding energy of 0.92 eV) than to interact with the hydroxylated surface.

The hydroxyls can effectively interact with each other on the surface, which results in an energy penalty for orienting to interact with water.

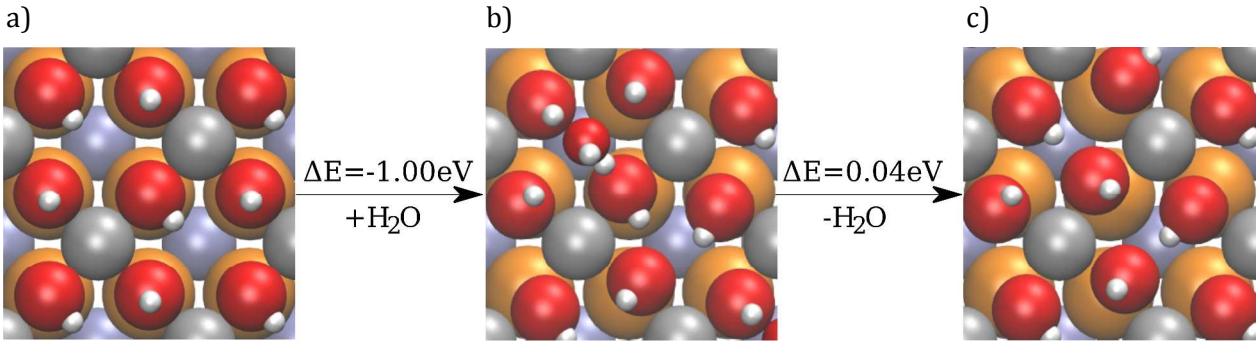

Figure 13. Water adsorption and desorption on the fully hydroxylated (100) ceria surface; radii and coloring as in Figure 11.

Discussion

Inferences on the electron-proton interaction in ^{1}H NMR spectra of nanocubes. The parameters contributing ^{1}H chemical shifts of hydroxyl groups (-OH) on metal oxides relevant to catalysis have been reviewed.[75] The diamagnetic shielding contribution from the electron density around the proton is the dominant term controlling the chemical shift of the hydroxyl proton in diamagnetic solids. Secondary perturbations include local magnetic anisotropy effects, proximity to electrically charged particles or ions, hydrogen bonding of the proton to surface functionality, and proton acidity.

For ceria, the manifestation of the electron–nuclear interaction, i.e., the e-^{1}H dipole–dipole interaction must be evaluated. Cerium in CeO_2 is in the +4 oxidation state and diamagnetic. However, the facile reducibility of ceria means that ceria may have some Ce^{+3} concentration, depending on sample history. For example, it is possible to partially reduce

ceria by moderate heating (300-500 °C) in vacuum. [12] The loss of a lattice oxygen creates an oxygen vacancy and two Ce^{+3}, each an unpaired electron center. The concentration of Ce^{+3} sites in nanoparticles can be estimated by Ce 3*d* XPS [76] and EPR measurements.[12] The concentration of Ce^{+3} sites increases as the particle size decreases, with the concentration increasing rapidly with particle sizes below 10 nm.[76] A nanocube particle size distribution of 20-100 nm results from the synthetic method used in this work[11]. On this basis the nanocubes are expected to contain a low concentration of Ce^{+3} centers. The e-^{1}H dipolar interaction introduces a mechanism to broaden and shift nuclear resonances within the electron sphere of influence.[77] Broadening has been observed previously by Fierro et. al. [13] in static ^{1}H NMR spectra of ceria samples heated in vacuum. In those studies, as 95% of the surface ^{1}H signal was eliminated as water by evacuating the sample between RT and 300 °C, the linewidth of the remaining signal narrowed. The full width at half height of the resonance, FWHH, decreased from ca. 20 to 14 kHz as the temperature increased from 20 to 300 °C. As the temperature was raised from 300 to 500 °C, FWHH increased to ca. 23 kHz. (The second moments of 4, 2, and 5 G^2 (field units) at 20, 300 and 500 °C, respectively, estimated from Figure 3c in reference 13, were converted to the stated FWHH values (frequency units) assuming a Gaussian lineshape.) The narrowing trend was attributed to a decrease in ^{1}H-^{1}H dipolar coupling as the surface density of –OH decreased: the subsequent broadening was attributed to the formation of paramagnetic centers as a consequence of partial surface reduction through the loss of lattice oxygen, and an increase in linewidth from e-^{1}H dipolar coupling. [13] Electron-proton dipolar coupling of this order will appear as weak sidebands in 40 kHz MAS ^{1}H spectra. We have already commented on sideband intensity of the proton resonances as indicating weak, ~10 kHz, dipolar coupling.

The 10-15% of the ^{1}H centerband resonance area in the first sideband pair at 10 kHz MAS reflect both weak e-^{1}H and ^{1}H-^{1}H dipolar coupling (Figure 10).

Fermi contact shifts (through bond coupling) on the order of 40 kHz recently have been reported between the electron on Ce^{3+} and directly bound lattice oxygen in the ^{17}O NMR spectrum of ceria nanoparticles. [70] Pseudo contact shifts and half-height linewidths of oxygen resonances in the Ce^{3+} second co-ordination shell are one to two orders of magnitude smaller, on the order of 0-30 ppm and 500 Hz, respectively. [70] Pseudo contact shifts in the kHz range, scaled by the 7.5-fold larger gyromagnetic ratio of the proton relative to ^{17}O, are expected in ^{1}H NMR spectra for the e–^{1}H dipolar interaction of surface –OH bound to the Ce^{+3} center. A possible resonance that might represent these pseudo contact-shifted protons in the ^{1}H spectra of nanocubes is the low-intensity high-frequency resonance that extends the 9 ppm resonance band to ca 12 ppm. Our assignment of this band to strongly hydrogen-bonded –OH functionality rests on the similarity of its T_1 value (several seconds) to the other low field resonances. It is anticipated that the T_1 of protons near an unpaired electron site will be relaxed efficiently through e-^{1}H dipolar relaxation. Fast relaxation is not observed for this low-intensity high-frequency resonance (Table 2, caption). Hence, the e-^{1}H dipole-dipole interaction is not apparent in the 20-40 kHz MAS spectra of these ceria nanocubes.

One caveat remains. Typically, using the 1.2 mm MAS probe and the onepuldpth sequence, the proton background signal from the Torlon rotor parts and further removed probe surfaces is 100-fold larger than the signal from surface species on the ceria cubes, necessitating careful analysis in background removal. While the background signal has been characterized extensively and great care is exercised in its removal, a smooth-

structured resonance with FWHH on the order of 30 kHz or greater potentially could be missed by inadvertent removal as a background signal. Spin counting experiments were used to evaluate this possibility. The surface –OH coverage in Table 1 for as-received non-calcined nanocubes is 0.9 ± 0.2 ML, in excellent agreement with DFT predictions (1 ML). Since the methodology results in –OH coverages that are essentially unity at RT, the exclusion of signal loss from e-^{1}H broadening is justified within the error limits of the measurement. The error estimates indicate that, in the worst case, no more than 20% of surface -OH could be missed due to broad resonances resulting from e-^{1}H interactions.

Surface Assignments. The assignments of nanocube resonances to –OH or water resonances follow from assessing the trends in ceria surface reactivity predicted by DFT calculations, chemical shift correlation, the relative strength of the proton dipole-dipole interaction at resolved sites in the ^{1}H spectra, comparative use of spin lattice relaxation times (T_1), and resonance response in water adsorption/desorption experiments. The assignments are summarized in Table 4.

The general trend that emerges from studies of neutral metal oxides (silica, titania) is that isolated surface –OH functions display a high field resonance that is shifted to lower field by hydrogen-bonding. The strong correlation between increasing hydrogen bond strength and increasing ^{1}H chemical shift (lower field shift) is well-established. [78] The hydrogen bond strength is mediated by distance and angle orientation within the hydrogen-bonded atoms. [78] This effect will lead to a heterogeneous distribution in chemical shifts depending on the constraints of solid surfaces. For example, the chemical shift of isolated SiOH on neutral silica appear at 1.7 ppm. Hydrogen-bonded silanols appear as a broad asymmetric resonance peaked at 3.0 ppm, with a low field tail that extends to 8.0 ppm. The low field

tail represents a continuously diminishing distribution of silanol protons involved in hydrogen bonds of increasing strengths. [67]

Table 4. Chemical shift assignment of resonance bands in ^{1}H MAS spectra of nanocubes.

Δ (ppm)	$\nu_{1/2}$ [a] (ppm)	Assignment	Comment
1	2	-OH	(100) surface [b], bridging hydroxyl, no (or exceedingly weak) hydrogen bond involvement
0.8, 1.2	0.5	-OH	(111) surface (corner bevels); no hydrogen bond involvement
3	1-2	-OH or H_2O	Shoulder resonance on the 1ppm peak. Surface –OH very weakly hydrogen-bonded to lattice oxygen or to molecular water.
4-7	2-3	H_2O	Physisorbed water, loosely held, minimal surface interactions.
9	5	-OH	(100) surface, strong hydrogen bonds to the lattice oxygen generating multiple resonance bands from 7 to 12 ppm
8.21 8.57	0.3 0.3	-OH -OH	Subsurface –OH, kinetically trapped during particle synthesis.

9.16	0.3	-OH	
9.65	0.3	-OH	Subsurface –OH, kinetically trapped during particle synthesis. Higher integrated intensity may indicate deeply buried –OH insensitive to surface features.

a) typical. b) the oxygen atom of all hydroxyl groups on the fully oxidized ceria <100> surface are bridging oxygens, associated with two second row cerium centers.

On the ceria (100) surface of cubes all surface –OH are bridging type, i.e., the oxygen is coordinated to two cerium centers. On the surface the orientation of the oxygen-proton bond of the hydroxyl function may be normal to the surface or may lie nearly in the plane of the top oxygen layer (Figure 13). In the former configuration no strong hydrogen bonds are possible with lattice-oxygen to hydroxyl-proton distances ≥2.5 Å; in the latter at least one strong hydrogen bond is found: d(OH) =1.87 Å, (see Figure 11d). Over the range of relaxed structures examined E_{ad} is similar, 1.67 ±0.04 eV, with the strongly hydrogen-bonded structure having the lowest energy. The inference is that the energy gain associated with the formation of strong hydrogen bonds adds to but is not the dominant driving force for increased surface stability.

The cube spectra, free of physisorbed water, display two prominent resonances bands, centered around 1 and 9 ppm (see Figure 7a, 8b). Isolated –OH are assigned to the 1 ppm, the ca. 2 ppm half-width reflecting the heterogeneity of the local surface structure. This assignment aligns with the 1.2 ppm chemical shift assigned to isolated -OH on a non-porous octahedral ceria (111) surface. [68, a]

Hydrogen-bonded hydroxyls on the ceria cube surface are assigned to the 9 ppm band. This band is asymmetric, beginning near 7 ppm and extending to 12 ppm (Figure 7, 8). Clear structure is seen within the band, a reflection of the crystallinity of the ceria and resultant discontinuous array of heterogeneously broadened hydrogen bond strengths. Unlike the ^{1}H NMR of silicas, the isolated and hydrogen-bonded surface –OH resonances on nanocubes are completely resolved, an indication that the surface can adjust to form an array of optimized hydrogen bonds. This likely results from the conformational disorder and fluxionality of oxygen surface species on the ceria (100) surface[7] that allows optimization of the hydrogen bond orientation and distance of surface -OH to lattice oxygen. The dominant feature of ^{1}H spectra of dry ceria cubes is the resolved 1 and 9 ppm resonance bands that reflect the collections of 'isolated' and hydrogen-bonded –OH on the surface, respectively. Spectra in Figure 7(b) and 8(a) are representative of this distribution on the dry cube surface, with the greater fraction of surface –OH in hydrogen-bonded configurations.

At low physisorbed water concentration a 3 ppm shoulder resonance on the 1 ppm resonance band is apparent (Figure 4(b), 5). The shoulder may represent the heterogeneity of the chemical shift range of isolated –OH due to variations in surface structure. This interpretation is the basis for the –OH designation in Table 4. Alternatively, the 3 ppm shoulder resonances may be due to weakly-bound molecular water associated with surface features. The water assignment is compatible with the observations presented in the next section, with the conjecture that the surface may present more than one motif.

Nanocubes with high sodium ion surface contamination: An exceptional case.

Nanocubes with excess Na^+ on the surface (from omitted ion exchange washing) and containing a physisorbed water resonance with intensity on the order of a ML possess exceptional spectra with a unique cluster of resolved resonances at 2.5-4 ppm (Figure 6). These resonances were interpreted in the Results section in the context of exchange averaging between surface bound and physisorbed water. These resonances nominally occupy the same chemical shift range as the 3 ppm shoulder resonance band in 'sodium-free' cubes and provide some justification for the assignment of the latter to water. They appear with high integrated intensity relative to the 9 ppm resonance band (cf. Figure 6(a) with Figure 4(b) and Figure 5). The high intensity of these resonances requires a proton source external to the surface and this can only be physisorbed water. In sodium-contaminated samples, the water may be drawn to the surface by interaction with the polar CeO^-Na^+ functionality that enhances the surface hydrophilicity. The existence of multiple, partially-resolved resonances within the high field band of Figure 6(a) suggests that molecular water exists in a few ordered configurations on the surface.

We argue below that molecular water does not normally exist in a weakly hydrogen-bonded state over a nominally hydroxylated, ion free, ceria (100) surface, but the small shoulder resonances in the spectra of the pristine dry cubes may belie the exclusivity of this claim, or rather, point out that a single, uniform description of the surface is overly simple. The assignment of the shoulder resonances in vacuum dried ceria cubes remains tentative for this reason.

The sharp low field resonances: synthesis artifacts. The last group of resonances in Table 4 is the four sharp peaks grouped between 8.21- 9.65 ppm. We conclude from the similarity in chemical shift and spin-lattice relaxation times that the sharp resonances do not differ in kind from the broader underlying resonances. Hence, they are assigned to hydrogen-bonded -OH isolated from water, i.e., -OH hydrogen-bonded to lattice oxygen. They are also similar to the 9 ppm peak in that none will exchange with deuterium by washing in D_2O under neutral, acidic or basic conditions. They are distinguished from the 9 ppm resonance band by four characteristics: 1) their unique highly reproducible chemical shifts, 2) their sharp linewidths, 3) the complete absence of sideband intensity at all MAS speeds, and 4) the fact that they are irreversibly eliminated from the spectra by mild (160 °C) heating under vacuum, and cannot be repopulated. The well-defined, highly reproducible chemical shifts demand that the resonances derive from four specific configurations within the crystal. The weak side band intensity at 10 kHz MAS reflects the average proton-proton distance of several Å and is the basis for assigning the 1 and 9 ppm resonance band to –OH. Still weaker ^1H-^1H dipolar coupling associated with the sharp resonances requires an even greater proton-proton separation for these species. On these bases, the four sharp resonances are assigned to thermodynamically unstable subsurface -OH within the cubic crystal lattice. DFT calculations indicate that subsurface hydrogen is energetically unfavorable by 1.6 eV. Kinetic trapping may offset this unfavorable energy during the particle's hydrothermal synthesis. An example of a dissociated water structure on the (100) surface, where one hydrogen is bound to third layer oxygen is depicted in Figure S9.

The four sharp peaks, while highly conspicuous in the spectra due to their very narrow linewidths, constitute a small fraction (4%) of the total ceria functionality. The most highly

populated resonance at 9.65 ppm has the longest T_1 among the sharp resonances. Speculation that this resonance derives from more deeply buried subsurface -OH with an environmentally insensitive chemical shift is not consistent with the interpretation of the T_1 data given above. The 9.65 resonance shows a bimodal T_1 dependence assigned to residual water and surface –OH. Within this interpretation, to invoke a distance dependence would require a T_1 with a trimodal dependence, not justified by the intensity data of the relaxation set. This indicates that the T_1 values of the resonances should not be interpreted with an overly simplistic (distance only) model.

An hydroxylated, hydrophobic nanocube surface. In the preceding discussion the ceria surface has been described as more or less hydrophobic. This description stems from two primary arguments: T_1 trends and ineffective deuterium exchange experiments. The T_1 values for physisorbed water and surface –OH are vastly different. The long T_1 component from surface –OH is insensitive to the hydration state of the ceria, remaining unchanged in as-received, non-calcined, or calcined cubes in wet and dry states. If the ^{1}H spin systems representing these two proton types were in intimate contact with each other, the T_1 values of the surface –OH would show averaged values by communication through spin diffusion. Furthermore, comparison of the values in Table 2 show the –OH values are also unaffected by washing the ceria in D_2O, an experiment meant to simulate the removal of the ^{1}H-^{1}H dipolar interaction between the two spin populations. More directly, the intensity of the ceria –OH resonances are unchanged in exchange experiments (D_2O washes) as shown in Figure 9. These results make sense if there is no close physical contact between the physisorbed water pool and surface ceria-OH functionality, i.e., the surface is hydrophobic. This counter-intuitive result applies to the hydroxylated surface. Ceria cubes that have

been carefully dried react with water with immediate dissociation to form the hydroxylated surface, as shown in Figure 8(d). Once formed the surface repels additional water, a result that implies the formation of strong hydrogen bonds between the surface –OH and lattice oxygen, such that there is no serious competition between surface –OH and physisorbed water. Figure 8d supports this conclusion, indicating the majority of surface –OH are strongly hydrogen bonded. The hydrophobic nature of the hydroxylated ceria surface gains some support from independent observations in a study of the interaction of D_2O with the ceria (100) surface investigated by temperature programmed desorption and X-ray photoelectron spectroscopy.[35] In that work, ceria (100) surfaces that have high concentrations of water, sufficient to form multilayers, show the O 1s emission from surface hydroxyl and substrate oxygen but do not record the O 1s emissions from deuterated water. That study suggested that this is due to the non-wetting behavior of water on the surface, with the formation of nanosized water clusters, three-dimensional beads of water above the ceria surface. Our DFT calculations affirm the notion that water may prefer to participate in hydrogen-bonded networks to other water molecules rather than interact with the hydroxylated surface with optimized surface -OH hydrogen bonding depicted in Figure 13(c).

Conclusions:

The (100) surface of ceria nanocubes contains two populations of surface –OH characterized primarily by their involvement (9 ppm resonance band, 5 ppm breadth, structured) or lack of involvement (1 ppm resonance band, 3 ppm FWHH, Gaussian) in

hydrogen bond formation to surface lattice oxygen. These resonances possess non-overlapping chemical shifts and characteristic spin lattice relaxation times. The hydroxyl population at room temperature is 0.9 ±0.2 ML, i.e., essentially a fully hydroxylated surface, consistent with DFT prediction. While the bands do present evidence of heterogeneous dispersion that reflect surface irregularities (oxygen vacancies, step edges, beveled edges) this dispersion is small, on the order of 1 ppm, permitting the observation of multiple resonance bands in solid-state ^{1}H spectra, assigned to water and surface –OH groups. Weak ^{1}H-^{1}H dipolar coupling characterizes all sites, eliminating strongly bound water as a surface component on ceria nanocubes.

The 9 ppm resonance band displays partially-resolved components representing strong surface –OH hydrogen-bond interactions in a limited number of configurations with lattice oxygens. Four sharp resonances superpose the low field band and arise from kinetically trapped subsurface –OH in unique internal environments. The lowest field resonance (9.65 ppm) may represent more deeply-buried –OH, with a chemical shift unaffected by surface boundary effects.

The hydroxylated ceria nanocube (100) surface is hydrophobic. This counterintuitive conclusion is demonstrated by the inability to exchange surface –OH for –OD in D_2O washing experiments and the complete insensitivity of the surface -OH spin lattice relaxation times as a function of drying. Both measures show that there is little communication between the protons in the physisorbed water and the surface –OH functionality. Following an initial adsorption and barrierless dissociation of water on the dry ceria nanocube surface, occurring first at oxygen vacancies, most surface –OH form hydrogen bonds to lattice oxygen so effectively that excess physisorbed water energetically

prefers to hydrogen bond to itself. The fluxional nature of the ceria surface, as judged by its easy redox and oxygen migration properties, likely allows effective distance and angle optimization of hydrogen bonds formed from –OH to lattice oxygen. This interpretation gains support from DFT calculations that indicate that the interaction of water with a fully hydroxylated surface is a thermoneutral process.

Acknowledgments:

This research was supported by the U. S. Department of Energy, Office of Basic Energy Sciences, Chemical Sciences, Geosciences, and Biosciences. The computational part of this project (AB) was conducted at the Center for Nanophase Materials Sciences under a user proposal. The Center is sponsored at Oak Ridge National Laboratory by the Scientific User Facilities Division, Office of Basic Energy Sciences, U.S. Department of Energy. This research used resources of the National Energy Research Scientific Computing Center, a DOE Office of Science User Facility supported by the Office of Science of the U.S. Department of Energy under Contract No. DE-AC02-05CH11231.

Supplemental Information

Fig. S1 Construction details of the adamantane packed end cap (adamcap).

Fig. S2 Pulse sequence for inversion-recovery T_1 measurements using a DEPTH filter for background removal: data set showing the spectra with residual background subtracted.

Fig. S3-S7 and Table S1 Spin Counting: quantitative surface coverage analysis.

Fig. S8 Stack plot of ^{1}H variable MAS spectra of a commercial ceria sample.

Fig. S9 A possible subsurface configuration for –OH in ceria.

References:

(1) Binet, C.; Daturi, M.;. Lavalley, J.-C; IR Study of Polycrystalline Ceria Properties in Oxidised and Reduced States *Catalysis Today* **1999**, *50* 207-225.

(2) Trovarelli, A. ; Leitenburg, C. D.; Boaro, M.; Docetti, G. The Utilization of Ceria in Industrial Catalysis, *Catalysis Today* **1999**, *50*, 353-367.

(3) Gorte, R. J.; Vohs, J. M. Catalysis in solid oxide fuel cells, *Ann. Rev. Chem. Biomol. Eng.* **2011**, *2*, 9-30.

(4) Sun, C.; Li, H.; Chen, L. Nanostructured ceria-based materials: synthesis, properties, and applications, *Ener. Envir. Sci.* **2012**, *5*, 8475-8505.

(5) Paier, J.; Penschke, C.; Sauer, J. Oxygen Defects and Surface Chemistry of Ceria: Quantum Chemical Studies Compared to Experiment, *Chem. Rev*. **2013**, *113*, 3949-3985.

(6) Gangopadhyay, S.; Frolov, D. D.; Masunov, A. E.; Seal, S. Structure and properties of cerium oxides in bulk and nanoparticulate forms, *J. Alloys and Compounds* **2014**, *584*, 199-208.

(7) Mullins, D. R. The Surface Chemistry of Cerium Oxide, *Surf. Sci. Rep*. *2015*, *70*, 42-85.

(8) Badri, A.; Binet, C.; Lavalley, J.-C. An FTIR Study of Surface Ceria Hydroxy Groups During Redox Process with H_2, *J. Chem. Soc, Faraday Trans.* **1996**, *92*, 4669-4673.

(9) Force, C.; Roman, E.; Guil, J. M.; Sanz, J. XPS and ^{1}H NMR Study of Thermally Stabilized Rh/CeO_2 Catalysts Submitted to Reduction/Oxidation Treatments, *Langmuir* **2007**, *23* 4569-4574.

(10) Madier, Y.; Descorme, C.; Le Govic, A.M.; Duprez, D. Oxygen Mobility in CeO_2 and $Ce_XZr_{(1-X)}O_2$ Compounds: Study by CO Transient Oxidation and $^{18}O/^{16}O$ Isotopic Exchange, *J. Phys. Chem. B* **1999**, *103*, 10999-11006.

(11) Wu, Z.; Li, M.; Howe, J.; Meyer, H. M. 3rd;, Overbury, S. H. Probing defect sites on CeO2 nanocrystals with well-defined surface planes by Raman spectroscopy and O2 adsorption, *Langmuir* **2010**, *26*, 16595-16606.

(12) Dutta, P.; Pal, S.; Seehra, M. S.; Shi, Y; Eyring, E. M.; Ernst, R. D. Concentration of Ce^{3+} and Oxygen Vacancies in Cerium Oxide Nanoparticles, *Chem. Mater.*. **2006**, *18*, 5144-5146.

(13) Fierro, J. L. G.; Soria, J. A.; Sanz, J.; Rojo, J. M. Induced Changes in Ceria by Thermal Treatments under Vacuum or Hydrogen, *J. Sol. State Chem*. **1987**, *66* 154-162

(14) Zafiris, G. S.; Gorte, R. J. Evidence for Low-Temperature Oxygen Migration from Ceria to Rh, *J. Catal.* **1993**, *139*, 561-567.

(15) Conesa, J. C.; Computer Modeling of Surfaces and Defects on Cerium Dioxide, *Surface Science* **1995**, *339*, 337-352.

(16) Botu, V.; Ramprasad, R.; Mhadeshwar, A. B. Ceria in an Oxygen Environment: Surface Phase Equilibria and its Descriptors, *Surface Science* **2014**, *619*, 49-58.

(17) Kim, H. Y.; Henkelman, G. CO Oxidation at the Interface between Doped CeO_2 and Supported Au Nanoclusters, *J. Phys. Chem. Lett.* **2012**, *3*, 2194-2199.

(18) Wu, Z.; Li, M.; Overbury, S.H. On the Structure Dependence of CO Oxidation over CeO_2 Nanocrystals with Well-defined Surface Planes, *Journal of Catalysis* **2012**, *285*, 61-73.

(19) Liu, Z.-G.; Chai, S.-H.; Binder, A.; Li, Y.-Y.; Ji, L.-T.; Dai, S. Influence of Calcination Temperature on the Structure and Catalytic Performance of CuOx-CoOy-CeO2 Ternary Mixed Oxide for CO Oxidation, *Applied Catalysis A: General* **2013**, *451*, 282-288.

(20) Agarwal, S.; Lefferts, L.; Mojet, B. L.; Ceria Nanocatalysts: Shape Dependent Reactivity and Formation of OH, *ChemCatChem* **2013**, *5*, 479-489.

(21) Agarwal, S.; Lefferts, L.; Mojet, B. L.; Ligthart, D. A. J. M.; Hensen, E. J.M.; Mitchell, D. R. G.; Erasmus, W. J.; Anderson, B. G.; Olivier, E. J.; Neethling, J. H.; Datye, A. K. Exposed Surfaces on Shape-Controlled Ceria Nanoparticles Revealed through AC-TEM and Water-Gas Shift Reactivity, *ChemSusChem* **2013**, *6*, 1898-1906.

(22) Bunluesin, T.; Gorte, R. J.; Graham, G. W. Studies of Water-Gas-Shift Reaction on Ceria-Supported Pt, Pd, and Rh: Implications for Oxygen-Storage Properties *Appl. Catal. B: Environmental* **1998**, *15*, 107-114.

(23) Chen, B.; Ma, Y.; Ding, L.; Xu, L.; Wu, Z.; Yuan, Q.; Huang, W. Reactivity of Hydroxyls and Water on a CeO2(111) Thin Film Surface: The Role of Oxygen Vacancy *J. Phys. Chem. C* **2013**, *117*, 5800-5810.

(24) Mullins, D.R.; Albrecht, P. M.; Chen, T.-L.; Calaza, F. C.; Biegalski, M. D.; Christen, H. M.; Overbury, S. H. Water Dissociation on CeO_2(100) and CeO_2(111) Thin Films *J. Phys. Chem. C* **2012**, *116*, 19419-19428.

(25) Senanayake, S. D.; Stacchiola, D.; Rodriguez, J. A. Unique Properties of Ceria Nanoparticles Supported on Metals: Novel Inverse Ceria/Copper Catalysts for CO Oxidation and the Water-Gas Shift Reaction, *Accounts of Chemical Research* **2012**, *46*, 1702-1711.

(26) Cargnello, M. ; Fornasiero, P.; Gorte, R. J. Opportunities for Tailoring Catalytic Properties Through Metal-Support Interactions, *Catalysis Letters* **2012**, *142*, 1043-1048.

(27) Akita, T.; Kohyama, M.; Haruta, M. Electron Microscopy Study of Gold Nanoparticles Deposited on Transition Metal Oxides, *Accounts of Chemical Research* **2012**, *45,* 1773-1782.

(28) Campbell, C.T. The Energetics of Supported Metal Nanoparticles: Relationships to Sintering Rates and Catalytic Acitvity, *Accounts of Chemical Research* **2013**, *46*, 1712-1719.

(29) Ma, Z.; Dai, S.; Design of Novel Structured Gold Nanocatalysts, *ACS Catalysis* **2011**, *1*, 805-818.

(30) Tana: Zhang, M.; Li, J.; Li, H.; Li, Y.; Shen, W. Morphology-dependent redox and catalytic properties of CeO2 nanostructures: Nanowires, nanorods and nanoparticles, *Catalysis Today* **2009**, *148*, 179-183.

(31) Fernández-Torre, D.; Kośmider, K.; Carrasco, J.; Ganduglia-Pirovano, M. V.; Pérez, R. Insight in to the Adsorption of Water on the Clean CeO_2 (111) Surface with van der Waals and Hybrid Density Functionals *J. Phys. Chem. C*, **2012**, *116*, 13584-13593.

(32) Molinari, M.; Parker, S. C.; Sayle, D. C.; Islam, M. S. Water Adsorption and Its Effect on the Stability of Low Index Stoichiometric and Reduced Surfaces of Ceria *J. Phys. Chem. C*, **2012**, *116*, 7073-7082.

(33) Mullins, D. R.; Albrecht, P. M.; Calaza, F. C., Variations in Reactivity on Different Crystallographic Orientations of Cerium Oxide, *Topics in Catalysis* **2013**, *56,* 1345-1362.

(34) Kundakovic, L.; Mullins, D. R.; Overbury, S. H., Adsorption and reaction of H_2O and CO on oxidize and reduced Rh/CeOx(111) surfaces, *Surf. Sci.* **2000**, *457(1-2)*, 51-62.

(35) Herman, G. S.; Kim, Y. J.; Chambers, S. A.; Peden, C. H. F. Interaction of D_2O with CeO_2(001) Investigated by Temperature-Programmed Desorption and X-ray Photoelectron Spectroscopy *Langmuir,* **1999**, *15*, 3993-3997.

(36) Fronzi, M.; Piccinin, S.; Delley, B.; Traversa, E.; Stampfl, C., Water adsorption on the stoichiometric and reduced CeO2(111) surface: a first-principles investigation, *Physical Chemistry Chemical Physics* **2009**, *11(40)*, 9188-9199.

(37) Kumar, S.; Schelling, P. K., Density functional theory study of water adsorption at reduced and stoichiometric ceria (111) surfaces, *J. Chem. Phys.*, **2006,** *125(20)*,

(38) Badri, A.; Binet, C.; Lavalley, J. C., An FTIR study of surface ceria hydroxy groups during a redox process with H-2, *J. Chem. Soc.-Faraday Trans*. **1996**, *92(23)*, 4669-4673.

(39) Hansen, H. A.; Wolverton, C. Kinetics and Thermodynamic of H_2O Dissociation on Reduced CeO_2(111) *J. Phys. Chem. C*, **2014**, *118*, 27402-27414.

(40) Wang, Y.-G.; Mei, D.; Li, J. & Rousseau, R. DFT+U Study on the Localized Electronic States and Their Potential Role During H_2O Dissociation and CO Oxidation Processes on CeO_2(111) Surface *J. Phys. Chem. C*, **2013**, *117*, 23082-23089.

(41) Fuente, S.; Branda, M. M.; Illas, F. Role of step sites on water dissociation on stoichiometric ceria surfaces *Theor. Chem. Acc*., **2012**, *131*, 1190

(42) Marrocchelli, D.; Yildiz, B. First-Principles Assessment of H_2S and H_2O Reaction Mechanisms and the Subsequent Hydrogen Absorption on the CeO_2(111) Surface *J. Phys. Chem. C*, **2012**, *116*, 2411–2424.

(43) Mai, H. X.; Sun, L. D.; Zhang, Y .W.; Si, R.; Feng, W.; Zhang, H.P.; Liu, H.C., Yan, C. H. Shape-Selective Synthesis and Oxygen Storage Behavior of Ceria Nanopolyhedra, Nanorods, and Nanocubes, *J. Phys. Chem. B*, **2005**, *109*, 24380-24385.

(44) Gines, M. J. L.; Iglesia, E.; Bifunctional Condensation Reactions of Alcohols on Basic Oxides Modified by Copper and Potassium *J. Catal.* **1998**, *176*, 155-172.

(45) Mann, A. K. P.; Wu, Z.; Calaza, F. C.; Overbury, S. H., Adsorption and Reaction of Acetaldehyde on Shape-Controlled CeO_2 Nanocrystals: Elucidation of Structure-function Relationships, *ACS Catalysis* **2014**, *4*, 2437−2448.

(46) Blochl, P. E. Projector Augmented-Wave Method *Phys. Rev. B*, **1994**, *50*, 17953–17979.

(47) Kresse, G.; Joubert, D. From Utrasoft Pseudopotentials to the Projector Augmented-Wave Method *Phys. Rev. B,* **1999**, *59*, 1758–1775.

(48) Kresse, G.: Hafner, J. Ab Initio Molecular Dynamics for Liquid Metals *Phys. Rev. B*, **1993**, *47*, 558–561.

(49) Kresse, G.; Hafner, J. Ab Initio Molecular Dynamics Simulation of the Liquid-Metal-Amorphous-Semiconductor Transition in Germanium *Phys. Rev. B*, **1994**, *49*, 14251–14269.

(50) Kresse, G.; Furthmüller, J. Efficiency of Ab Initio Total Energy Calculations for Metals and Semiconductors Using a Plane-Wave Basis Set *Comput. Mat. Sci.*, **1996**, *6*, 15–50.

(51) Kresse, G.; Furthmüller, J. Efficient Iterative Schemes for Ab Initio Total Energy Calculations Using a Plane-Wave Basis Set *Phys. Rev. B*, **1996**, *54*, 11169–11186.

(52) Paier, J.; Penschke, C. & Sauer, J. Oxygen Defects and Surface Chemistry of Ceria: Quantum Chemical Studies Compared to Experiment *Chem. Rev*., **2013**, *113*, 3949–3985.

(53) Perdew, J. P.; Burke, K.; Ernzerhof, M. Generalized Gradient Approximation Made Simple *Phys. Rev. Lett.*, **1996**, *77*, 3865–3868.

(54) Dudarev, S. L.; Botton, G. A.; Savrasov, S. Y.; Humphreys, C. J. & Sutton, A. P. Electron-Energy-Loss Spectra and the Structural Stability of Nickel Oxide: An LSDA+U Study *Phys. Rev. B*, **1998**, *57*, 1505–1509.

(55) Watkins, M. B.; Foster, A. S.; Shluger, A. L. Hydrogen Cycle on CeO_2 (111) Surfaces: Density Functional Theory Calculations *J. Phys. Chem. C*, **2007**, *111*, 15337–15341.

(56) Huang, M.; Fabris, S. CO Adsorption and Oxidation on Ceria Surfaces from DFT+U Calculations *J. Phys. Chem. C*, **2008**, *112*, 8643-8648.

(57) Loschen, C.; Carrasco, J.; Neyman, K. M.; Illas, F. First-principles LDA+U and GGA+U study of cerium oxides: Dependence on the effective U parameter *Phys. Rev. B*, **2007**, *75*, 035115-1–8.

(58) Calaza, F. C.; Xu, Y.; Mullins, D. R.; Overbury, S. H. Oxygen Vacancy-Assisted Coupling and Enolization of Acetaldehyde on CeO_2(111) *J. Am. Chem. Soc*., **2012**, *134,* 18034–18045.

(59) Beste, A.; Overbury, S. H. Hydrogen and Methoxy Coadsorption in the Computation of the Catalytic Conversion of Methanol on the Ceria (111) Surface *Surf. Sci*., **2016**, *648*, 242-249.

(60) Kropp, T.; Paier, J. Reactions of Methanol with Pristine and Defective Ceria (111) Surfaces: A Comparison of Density Functionals *J. Phys. Chem. C* **2014**, *118*, 23690-23700.

(61) Grimme, S.; Antony, J.; Ehrlich, S.; Krieg, H. A Consistent and Accurate ab initio Parametrization of Density Functional Dispersion Correction (DFT-D) for the 94 Elements H-Pu *J. Chem. Phys.*, **2010**, *132*, 154104-1-19.

(62) Herman, G. S. Surface Structure Determination of CeO_2(001) by Angle-Resolved Mass Spectroscopy of Recoiled Ions *Phys. Rev. B,* **1999**, *59*, 14899-14902.

(63) Nörenberg, H.; Harding, J. H. The Surface Structure of CeO_2(001) Single Crystals Studied by Elevated Temperature STM *Surf. Sci.*, **2001**, *477*, 17-24.

(64) Skorodumova, N. V.; Baudin, M.; Hermansson, K. Surface Properties of CeO_2 from First Principles *Phys. Rev. B*, **2004**, *69*, 075401-1-8.

(65) Jónsson, H.; Mills, G. & Jacobsen, K. W. Berne, B. J.; Ciccotti, G. & Coker, D. F. (Eds.) Classical and Quantum Dynamics in Condensed Phase Simulations Nudged Elastic Band Method for Finding Minimum Energy Paths of Transitions *World Scientific*, **1998**, *385*,

(66) http://theory.cm.utexas.edu/vtsttools/download.html

(67) Bronnimann, C. E.; Zeigler, R. C.; Maciel, G. E. Proton NMR-Study of Dehydration of the Silica-Gel Surface, *J. Amer. Chem. Soc.* **1988**, *110*, 2023-2026.

(68) Lyons, D. M.; McGrath, J. P.; Morris, M. A. Surface Studies and Mesoporous Ceria Powders by Solid-Sate ^{1}H NMR *J. Phys. Chem. B* **2003**, *107*, 4607-4617.

(69) Lin, Y.; Wu, Z; Wen, J.; Poeppelmeier, J. R.; Marks, L. D. Imaging the Atomic Surface Structures of CeO_2 Nanoparticles *Nano Lett.* **2014**, *14*, 191-196.

(70) Wang, M.; Wu, X.-P.; Zheng, S.; Zhao, L.; Li, L.; Shen, L.; Gao, Y.; Xue, N.; Guo, X.; Huang, W.; Gan, Z.; Blanc, F.; Yu, Z.; Ke, X.; Ding, W.; Gong, X.-Q.; Grey, C. P.; Peng, L.

Identification of Different Oxygen Species in Oxide Nanostructures with ^{17}O Solid-State NMR Spectroscopy, *Sci. Adv*. **2015**, 1:e1400133.

(71) Eckert, H.; Yesinowski, J. P.; Silver, L. A.; Stolper, E.M.; Water in Silicate Glasses - Quantitation and Structural Studies by H-1 Solid Echo and MAS-NMR Methods, *J. Phys. Chem.* **1988**, *92*, 2055-2064.

(72) Nolan, M. Hybrid Density Functional Theory Description of Oxygen Vacancies in the CeO_2 (110) and (100) Surfaces *Chem. Phys. Lett.*, **2010**, *499*, 126–130.

(73) Shannon, R. D. Revised Effective Ionic Radii and Systematic Studies of Interatomic Distances in Halides and Chalcogenides, *Acta Cryst.*, **1976**, *A32*, 751-767.

(74) Allen, F. H.; Kennard, O.; Watson, D. G.; Brammer, L.; Orpen, A. G. & Taylor, R. Table of Bond Lengths Determined by X-Ray and Neutron Diffraction *J. Chem. Soc., Perkin Trans.*, **1987**, *2*, S1–S19.

(75) V. M. Mastikhin, I. L. Mudrakovsky, A.V. Nosov, "^{1}H NMR Magic Angle Spinning (MAS) Studies of Heterogeneous Catalysis'', *Prog. NMR Spectr.* **1991**, *23*, 259-299.

(76) Deshpande, S.; Patil, S.; Kuchibhatia, S. V. N. T.; Seal, S. Size Dependency Variation in Lattice Parameter and Vacancy States in Nanocrystalline Cerium Oxide *Appl. Phys. Lett.* **2005**, *87*, 133113.

(77) Principles and Applications of ESR Spectroscopy, Anders Lund, Masuru Shiotani and Shigetaka Shimada, Springer, 2011. ISBN 978-1-4020-5343-6

(78) Berglund, B.; Vaughan, R. W. Correlations Between Proton Chemical Shift Tensors, Deuterium Quadrupole Couplings, and Bond Distances for Hydrogen Bonds in Solids *J. Chem. Phys*. **1980**, *73*, 2037-2043.

Table of Contents Graphic for:

Fast MAS ^{1}H NMR Study of Water Adsorption and Dissociation on the (100) Surface of Ceria Nanocubes: A Fully Hydroxylated, Hydrophobic Ceria Surface, Lance Gill, Ariana Beste, Banghao Chen, Meijun Li, Amanda K. P. Mann, Steven H. Overbury and Edward W. Hagaman *